DOCKET NO: A-93-02
V-B-8

TECHNICAL SUPPORT DOCUMENT for SECTION 194.23:

POTENTIAL EFFECTS OF MINING ON GROUND WATER FLOW AND RADIONUCLIDE TRANSPORT AT THE WIPP SITE

U.S. ENVIRONMENTAL PROTECTION AGENCY
Office of Radiation and Indoor Air
Center for the Waste Isolation Pilot Plant
401 M. Street, S.W.
Washington, DC 20460

MAY 1998

TABLE OF CONTENTS

1. Introduction 1-1

2. Mining Scenarios 2-1

3. Literature Review 3-1
3.1 WIPP Related Studies 3-1
3.1.1 Final Environmental Impact Statement 3-1
3.1.2 D'Appolonia Studies 3-1
3.1.3 IT Corporation Backfill Engineering Analysis 3-3
3.1.4 SNL Studies of Subsidence 3-6
3.2 Other Relevant Studies 3-6
3.2.1 New Mexico Potash Mines 3-6
3.2.2 Coal Mines 3-7

4. Impact of Mining on Hydraulic Conductivity 4-1
4.1 Background Information 4-1
4.2 Strain Analysis 4-8
4.2.1 Finite Element Analysis 4-8
4.2.1.1 Material Properties 4-8
4.2.1.2 Geologic Column 4-9
4.2.1.3 Mining Geometry 4-11
4.2.1.4 Premining Stress State 4-11
4.2.1.5 Boundary Conditions 4-11
4.2.2 Fracture Conductivity Change 4-14
4.2.3 Strain Analysis Results 4-15
4.2.3.1 Case 1 (Substance Factor of 52.5%). 4-15
4.2.3.2 Case 2 (Subsidence Factor of 67.5%) 4-21
4.3 Flow and Transport Studies 4-27
4.3.1 Introduction 4-27
4.3.2 Problem Conceptualization 4-28
4.3.3 Model Formulation 4-32
4.3.3.1 Homogeneous Hydraulic Conductivity Simulations 4-32
4.3.3.2 Heterogeneous Hydraulic Conductivity Simulations 4-35
4.3.4 Description of Simulations 4-42
4.3.4.1 Comparison of Homogeneous Simulations 4-43
4.3.4.2 Comparison of Heterogeneous Hydraulic Conductivity Simulations . . . 4-57
4.3.4.3 Comparison Between Homogeneous and Heterogeneous Simulations . . 4-66

TABLE OF CONTENTS
(continued)

5. Consideration of Other Mining Impacts 5-1
5.1 Solution Mining 5-1
5.2 Change in Flow Direction of Water-Bearing Members if Vertical Hydraulic Connection is Created by Subsidence 5-2
5.3 Formation of Subsidence-Related Surface Depressions Where Water Could Accumulate and Alter Local Recharge 5-2
5.4 Increased Hydraulic Gradient if Significant Flow From Water-Bearing Strata into Mine Workings Occurs 5-2
5.5 Damage to Borehole or Shaft Seals by Subsidence . . . 5-7
5.6 Increased Hydraulic Conductivity of the Salado Formation Due to Excavation-Induced Stresses 5-8

6. Difference Between Ground-Water Modeling Studies in this Report and in CCA 6-1

7. Summary 7-1

8. References 8-1

Figures

1-1. Generalized Stratigraphic Column of Permian and Younger Strata, Eddy County, New Mexico (CHE78) 1-3
1-2. Location of BLM Lease Grade Mineralization Within the WIPP Site (GRI95 1-4
1-3. Outline of the Designated Potash Area, KPLA, Area of Leasable Reserves and Mined-Out Areas within Delaware Basin (BLM93) . . . 1-9

4-1. Finite Element Mesh Used for Strain Analysis Mesh 4,500 ft by 6,750 ft 4-12
4-2. Half Width (1,500 ft) of Mined Panel 4-13
4-3. Subsidence-induced Culebra strains for subsidence factor of 52.5%. (Panel extends +/-1,500 ft from origin) 4-16
4-4. Aperture Change in Vertical Joints for Fracture Spacings of 3, 30, and 300 inches and Subsidence Factor of 52.5% 4-18
4-5. Aperture Change in Horizontal Joints for Fracture Spacings of 3, 30, a 300 inches and a Subsidence Factor of 52.5% 4-18
4-6. Relative Change in Fracture Hydraulic Conductivity for Vertical Joints with Various Fracture Spacings, Subsidence Factor of 52.5%, and Fractu Apertures of 10^{-4}, 10^{-3}, and 10^{-2} in. a) 3 inch b) 30 inch c) 300 inch Spacing 4-19
4-7. Relative Change in Fracture Hydraulic Conductivity for Horizontal Join with Various Fracture Spacings, Subsidence Factor of 52.5%, and Fractu Apertures of 10^{-4}, 10^{-3}, and 10^{-2} in. a) 3 inch b) 30 inch c) 300 inch Spacing 4-20
4-8. Subsidence-induced Culebra Strains for Subsidence Factor of 67.5% (Panel extends +/-1,500 ft from origin) 4-22
4-9. Subsidence-induced Culebra Strains for Subsidence Factor of 67.5%. (Panel extends +/-1,500 ft from origin.) Horizontal Mesh Extended to 13,500 ft. 4-22
4-10. Aperture Change in Vertical Joints for Fracture Spacings of 3, 30, and 300 inches and Subsidence Factor of 67.5% 4-23
4-11. Aperture Change in Horizontal Joints for Fracture Spacings of 3, 30, a 300 inches and a Subsidence Factor of 67.5% 4-23
4-12. Relative Change in Fracture Hydraulic Conductivity for Verticle Joints with Various Fracture Spacings, Subsidence Factor of 67.5%, and Fractu Apertures of 10^{-4},10^{-3}, and 10^{-2} in. a) 3 inch b) 30 inch c) 300 inch Spacings 4-25

4-13. Relative Change in Fracture Hydraulic Conductivity for Horizontal Join with Various Fracture Spacings, Subsidence Factor of 67.5%, and Fractu Apertures of 10^{-4},10^{-3}, and 10^{-2} in. a) 3 inch b) 30 inch c) 300 inch Spacings 4-26
4-14. Equivalent Porous Matrix Hydraulic Conductivity Computed for a Strain of 0.005% 4-36
4-15. Composite Transmissivity Field from Intera (Log_{10} T m^2/s) 4-37
4-16. Interpolated Transmissivity Distribution (Log_{10} T m^2/s) 4-38
4-17. Unstrained Hydraulic Conductivity Distribution (m/y) over WIPP Site 4-41
4-18. Strain Altered Hydraulic Conductivity Values Over WIPP Site for 1 Fracture 4-44
4-19. Strain Altered Hydraulic Conductivity Values Over WIPP Site for 10 Fractures 4-45
4-20. Strain Altered Hydraulic Conductivity Values Over WIPP Site for 100 Fractures 4-46
4-21. Unstrained Homogenous Hydraulic Conductivity Simulations Without Physical or Chemical Retardation 4-50
4-22. Strained and Unstrained Homogenous Hydraulic Conductivity Simulations Without Physical or Chemical Retardation 4-52
4-23. Homogenous Hydraulic Conductivity Simulations with Physical Retardation 4-54
4-24. Homogeneous Hydraulic Conductivity Simulations with High and Low Value of Diffusion 4-56
4-25. Homogeneous Hydraulic Conductivity Simulations Comparing the Effects o Physical and Chemical Retardation on Radionuclide Transport Times 4-58
4-26. Homogeneous Hydraulic Conductivity Simulations that include Physical a Chemical Retardation 4-59
4-27. Contaminant Plume for the Heterogeneous Simulation after 61,000 Years 4-61
4-28. Heterogeneous Hydraulic Conductivity Simulations without Physical or Chemical Retardation 4-62
4-29. Heterogeneous Hydraulic Conductivity Simulations with Physical Retardation 4-65
4-30. Heterogeneous Hydraulic Conductivity Simulations Comparing the Effects of Physical and Chemical Retardation on Radionuclide Transport Times 4-67

4-31.Heterogeneous Hydraulic Conductivity Simulation with Physical and Chemical Retardation 4-69

5-1. The ratio of the hydraulic gradient imposed by mining to the ambient gradient 5-6

Tables

1-1. Potash Reserves and Resources Within WIPP Site Boundary (CRT95) 1-5
1-2. Active Potash Mines in New Mexico Showing Estimated Capacity, Average Ore Grade, and Mine Life at the Average 1992 Price of $81.14/st produc 1-7

3-1. Summary of IT Corp. Subsidence Prediction Results for WIPP Repository (ITC94) 3-5

4-1. Rock Properties By Type 4-9
4-2. Strata Depth and Thickness at WIPP Site 4-10
4-3. Hydraulic Conductivities and Fracture Porosity for Homogeneous Simulations 4-33
4-4. Input Parameters for Homogeneous Hydraulic Conductivity Simulations 4-34
4-5. Hydraulic Conductivities and Porosity Values Used in Heterogeneous Simulations 4-41
4-6. Input Parameters for Heterogeneous Hydraulic Conductivity Simulations 4-42
4-7. Summary of Concentration Breakthrough at a Distance of 2.4 km Downgradient of the Source (WIPP Land Withdrawal Boundary) 4-47
4-8. Selected Results from Homogeneous Hydraulic Conductivity Simulations Without Physical or Chemical Retardation 4-49
4-9. Selected Results from Homogeneous Hydraulic Conductivity Simulations with Physical Retention 4-57
4-10. Selected Results from Homogeneous Hydraulic Conductivity Simulations with Physical and Chemical Retardation 4-60
4-11. Selected Results from Heterogeneous Hydraulic Conductivity Simulations without Physical or Chemical Retardation 4-63
4-12. Selected Results from Heterogeneous Hydraulic Conductivity Simulations with Physical Retardation 4-66
4-13. Selected Results from Heterogeneous Hydraulic Conductivity Simulations with Both Physical and Chemical Retardation 4-68

5-1. Summary of Results for Mine Shaft Leakage Scenario . . . 5-4
5-2. Groundwater Velocities at Hydraulic Conductivities Ranging from 2-1000 Times Those Values Presented in Table 5-1 5-7

Technical support for this document was provided by Sandy Cohen and Associates, Inc. And/or its subcontractors under EPA Contract 68D70073.

1. Introduction

When considering the possible consequences of future human activities on sealed geologic repositories, scenarios involving drilling for resources are frequently modeled (GAL94, NEA92). However, in resource-rich areas, underground mining scenarios may also require modeling to define the full range of possible repository impacts. This report considers possible mining-related scenarios which might impact the integrity of the Waste Isolation Pilot Plant (WIPP) after closure. The report focuses on potash since this is the major mineral currently extracted in the Delaware Basin by underground mining. Economic deposits of potash are confined to the northern portion of the Basin in Eddy and Lea Counties, New Mexico near the WIPP site. No other significant underground mining occurs in the Delaware Basin, although some sulfur is extracted via Frasch process wells (in the Castile Formation) in Culberson County, Texas (POW78).

Potash is a general term for a variety of potassium bearing minerals for which the chemical compound K_2O is often used as a surrogate to characterize the potassium content. About 95% of U.S. potash sales are to the fertilizer industry with the balance primarily to the chemical industry. Historical sources of potash include kelp, wood ashes, lake brines, alunite, cement dust, sugar beet waste, blast furnace dust, and various potassium-rich minerals. Today, U.S. potash production is principally from the rock sylvinite - a mixture of the minerals sylvite (KCl) and halite (NaCl) - and from langbeinite - a potassium magnesium sulfate ($K_2SO_4 \bullet 2MgSO_4$). Potash is typically recovered either by underground excavation mining or by solution mining where water is injected into a mineralized zone and saturated brine is extracted and recrystallized in evaporation ponds. In the Delaware Basin, potash is recovered only by excavation mining.

Extensive underground potash mining is currently being conducted in the vicinity of the WIPP site. During 1992, southeastern New Mexico supplied 81% of U.S. production (DUP94). Mining operations occur in the McNutt potash zone[1] of the Salado Formation. A generalized stratigraphic column showing these Upper Permian potash-bearing rocks and younger, over-lying strata is included as Figure 1-1 (CHE78). Eleven ore zones have been identified within the McNutt. Primary current mining targets are the 10th ore zone for sylvite and the 4th ore zone for langbeinite. Some mineralization has been identified in ore

[1] This is sometimes referred to in the literature as the McNutt Member of the Salado Formation.

zones 2, 3, 5, 8, 9, and 11 in the WIPP vicinity[2](NMB95). The depth of the 11 identified ore zones in the McNutt, based on the ERDA-9 borehole, ranges from about 1,372 feet to 1,741 feet near the WIPP site (POW78) and the McNutt dips generally to the east (CHE78). The ore zones vary widely in thickness and mineralization and are often not continuous. Even when mineralization is present in an ore zone, it may not be sufficient to be of commercial interest. In some cases, mineralization is absent altogether. Since the WIPP repository is located in the Salado at a depth of 2,150 feet, the deepest potash resources are about 400 feet above and laterally removed from the waste repository.

The mineralized zones extend within the WIPP Land Withdrawal Boundary as shown in Figure 1-2 which plots the boundaries of the current Bureau of Land Management (BLM) Lease Grade criteria[3] and minable reserves as estimated by Griswold (GRI95). Reserve and resource estimates inside the WIPP boundary are summarized in Table 1-1 (NMB95). When the WIPP site was selected in 1976, most of the site lay outside the boundary of the Known Potash Leasing Area (KPLA) (i.e., the area which contains lease grade reserves). However, subsequent site evaluation by DOE (then ERDA) included drilling and coring 21 exploratory holes for potash (POW78). This drilling program indicated that potash mineralization was more extensive than previously expected. As a consequence, the U.S. Geological Survey used these drill hole data to extend the KPLA. The KPLA now embraces all of the WIPP site although most of the southwestern quadrant of the site is barren of mineralization, as is the repository location.

Leasable langbeinite reserves underlie 25% of the WIPP site as defined by the Land Withdrawal Boundary while leasable sylvite reserves underlie 40% of the WIPP site (Figure 1-1). Since there is some areal overlap of langbeinite and sylvite ore zones in the northeast corner of the site, the total area underlain by leasable potash is 54% of the WIPP site. Similarly, 8% of the site is underlain by minable langbenite and 22% by minable sylvite. The combined minable reserve area, adjusted for overlapping ore zones, is 29% of the total WIPP site.

---

[2] The New Mexico Bureau of Mines and Mineral Resources reserve and resource estimates are based on 40 drill holes in and around the WIPP site. Other drill holes exist in the area, but the data are proprietary. These 40 drill holes cover the WIPP Land Withdrawal area and an area extending about 1 mile outside the boundary except for the southwest quadrant of this perimeter area (GRI95).

[3] The current BLM leasing criteria for potash reserves specify ore seams containing at least 4 feet of 4% K_2O (a grade-thickness product of 16) for langbeinite and 4 feet of 10% K_2O for sylvite (a grade-thickness product of 40). These criteria have been in effect since 1969. According to BLM, sylvite is being mined below the 10% K_2O minimum cutoff grade and langbeinite is being mined below the 4% minimum (CON95).

Figure 1-1. Generalized Stratigraphic Column of Permian and Younger Strata, Eddy County, New Mexico (CHE78)

Figure 1-2. Location of BLM Lease Grade Mineralization Within the WIPP Site.

Table 1-1. Potash Reserves and Resources Within WIPP Site Boundary (GRI95)

AREA	TYPE OF RESOURCE	MILLION SHORT TONS	K_2O (%)
4th Ore Zone (Langbeinite)	In-place resource (>4% K_2O and actual thickness)	47.0	7.12
	BLM Lease Grade reserve (>4% K_2O and 4-foot mining height)	40.5	6.99
	Minable reserve (>6.25% K_2O and 6-foot mining height)	18.0	7.59
10th Ore Zone (Sylvite)	In-place resource (>10% K_2O and actual thickness)	53.7	14.26
	BLM Lease Grade reserve (>10% K_2O and 4-foot mining height)	52.3	13.99
	Minable reserve (>12.25% K_2O and 4.5 foot mining height)	30.6	15.00
Other Ore Zones	In-place resources[a]	18.4	5.74-15.71

a - Generally do not meet lease grade standards. According to GRI95, these resources could only be minable if advanced thin-seam mining techniques are developed in the future.

The WIPP site lies within what is called the Designated Potash Area. This area, which is defined by Order of Secretary of Interior (51 FR 39425) under the authority of two mineral leasing acts, is slightly larger than the KPLA. It should be noted that the northern most townships within the Designated Potash Area lie outside the northern boundary of the Delaware Basin.[4] According to the Secretarial Order, potash enclaves are delineated within the Designated Potash Area as regions containing currently economically minable ore reserves. Inside these enclaves, it is Department of Interior policy to deny approval of most oil and gas drilling permit applications from surface locations with two exceptions (51 FR 39425):

"a. Drilling of vertical or directional holes shall be allowed from barren areas within the potash enclaves when the authorized officer determines that such operations will not adversely affect active mining operations in the vicinity of the proposed drillsite.

b. Drilling of vertical or directional holes shall be permitted from a drilling island located within a potash enclave when: (1) There are no barren areas within the enclave or drilling is not permitted within on the established barren area(s) within the enclave because of interference with mining operations; (2) the objective oil and gas formation cannot be reached by a well which is vertically or directionally drilled from a permitted location within the barren area(s); or (3) in the opinion of the

[4] About 50% of the Designated Potash Area lies outside the Delaware Basin.

authorized officer, the target formation beneath a remote interior lease cannot be reached by a well directionally drilled from a surface location outside the potash enclave."

For perspective, the Designated Potash Area, as of October 1986, occupied about 497,000 acres (777 mi^2) as compared to the area of the WIPP site which is 10,240 acres (16 mi^2). Drilling on state and private lands is controlled by the New Mexico Oil Conservation Division (OCD). Because of problems in implementing then existing OCD regulations, a revised order (No. R-111-P) was approved by the State Oil Conservation Commission on April 21, 1988 (OCC88). Under the terms of R-111-P, the New Mexico "Potash Area" is coterminous with the KPLA. Within the Potash Area, drilling for oil and gas on state and private lands cannot be conducted at any location containing life-of-mine potash reserves (LMR) except by mutual agreement of the lessor and lessee of both the potash and oil and gas interests. Outside the LMR, drilling of shallow wells can be no closer than 0.25 miles of the LMR boundary or 110% of the ore depth, whichever is greater. (Shallow wells are defined as those in all formations above the base of the Delaware Mountain Group or less than 5,000 feet deep, whichever is less.) Deep wells must be at least 0.5 miles from the LMR boundary. One of the objectives of R-111-P was to eliminate the need for drilling islands and three-year mining plans required by the Secretarial Order on Federal lands.

Potash ore reserves in the KPLA were estimated to be about 100 million short tons (90.7 million metric tons) of recoverable K_2O based on 1973 prices (WEI79)[5]. At current production rates of about 1.4 million metric tons per year (DUP92), this reserve would be exhausted in about 65 years (about 15 years after projected completion of the WIPP disposal phase, but during the period of active institutional controls)[6]. In the 1993 WIPP Resource Disincentive Report, DOE commented on the finite nature of the langbeinite supply noting that langbeinite operations would continue for another 28 years if only current reserves are considered and the production period would be extended to 46 years if resources were also included (DOE93). In 1993, the New Mexico Bureau of Mines and Mineral Resources provided a breakdown of the expected operational life of each mine in the area. As shown in Table 1-2, life of the Mississippi Chemical operations is projected to be 125 years while the

[5] In a 1978 study, AIM Inc. estimated potash reserves for the Carlsbad District including those within the WIPP site to contain 109 million tons of recoverable products - a total very similar to the 1973 Bureau of Mines estimate (SEE78).

[6] In 1973, the U.S. Geological Survey stated that, based on then current production levels, crystalline deposits and brines in the U.S. would last for at least 100 years (SMI73). Nearby Canadian resources are adequate for thousands of years.

other five mines should wind down in 33 years or less (BAR93). It should be noted that the mine life estimates are based on published information. Data on actual mining reserves are regarded as proprietary information by the potash mining companies and actual mine life may be longer than projected here.

Table 1-2. Active Potash Mines in New Mexico Showing Estimated Capacity, Average Ore Grade, and Mine Life at the Average 1992 Price of $81.14/st product.

Operator	County	Product Capacity (st/yr[1])	Ore Grade (% K_2O)	Mine Life (yrs)
Eddy Potash Inc.[2]	Eddy	550,000	18	4
Horizon Potash Co.	Eddy	450,000	12	6
IMC Fertilizer, Inc.	Eddy	1,000,000[3]	11[3]	33
Mississippi Chemical	Eddy	300,000	15	125
New Mexico Potash[2]	Eddy	450,000	14	25
Western Ag-Minerals[4]	Eddy	400,000	8[5]	30

Data from J.P. Searls, U.S. Bureau of Mines, oral communication, 1993.
[1] May not be operating at full capacity.
[2] Owned by Trans-Resource, Inc.
[3] Muriate, langbeinite, and sulfate combined.
[4] Owned by Rayrock Resources of Canada.
[5] Langbeinite only.

Current mining operations can be economically extended to the WIPP site boundary and it is likely that this will occur (GRI95). Although economic mineralization also lies within the WIPP site as indicated in Table 1-1, the WIPP Land Withdrawal Act (LWA) (Public Law 102-579) precludes mining within the withdrawn area. However, at some future time, when active institutional controls no longer exist and if passive institutional controls are ineffective, mining of the potash inside the boundary is a conceptual possibility. The economics would, of course, be different and exploitation would probably require creation of a new infrastructure to transport ore to the surface and beneficiate it since existing facilities would have been abandoned. GRI95 estimates of minable reserves within the site boundary assume that new mine and plant facilities would not be needed if the reserves were exploited now. As described in Table 1-1, minable reserve estimates are based on higher grades and greater ore seam thicknesses than for Lease Grade reserves.

Potash was first produced from the Delaware Basin in 1931 (BAR93, GRI82). The Designated Potash Area covers an area of approximately 290 mi^2 in the Delaware Basin with the remainder of the areas located over the Capitan Reef or outside of the Delaware Basin.

Since 1931, mining of the different potash ore zones has covered an area in the Delaware Basin of over 40 mi^2 as estimated from a 1993 map of the potash resources (BLM93). Leasable reserves and mined out areas are shown in Figure 1-3.

Using 9700 mi^2 as the approximate area of the Delaware Basin, it can be estimated that about 0.4% of the Delaware Basin has been mined over the past 62 years (1931-1993). This produces a conservative estimate of the rate of mining of 1% of the Delaware Basin area over the past 100 years. Any mining of potash or other minerals of current interest elsewhere in the Delaware Basin would raise this percentage.

The following sections discuss potential impacts of mining on the anticipated long-term performance of the WIPP repository and elaborate on the position taken by EPA in the 40 CFR part 194 rule (§194.32(a)) that performance assessment shall consider the effects of mining on the disposal system and these effects can be limited to changes in the hydraulic conductivity of the disposal system induced by mining. Chapter 2 discusses possible mining scenarios, Chapter 3 discusses information gleaned from the literature on subsidence-issues related to underground mining, Chapter 4 presents an analysis of the impact of strains created in the overburden from mining subsidence on groundwater flow and radionuclide transport, Chapter 5 considers the impact of other mining related scenarios on the WIPP, Chapter 6 compares the ground-water modeling done for this report with that conducted by DOE for the WIPP Compliance Certification Application (CCA), and Chapter 7 summarizes the report.

A portion of this analysis was completed earlier and included in the 40 CFR part 194 Background Information Document (BID) (EPA 1996). This report includes an updating of that information as well as additional information developed subsequent to publication of this TSD.

Figure 1-3. Outline of the KPLA, (Area of Leasable Reserves), and Mined-Out Areas within Delaware Basin (BLM 93).

2. Mining Scenarios

Consideration of mining effects on performance assessment (PA) involves scenarios where mining occurs up to the land withdrawal boundary and where mining occurs within the withdrawn area up to the limits of economic mineralization. Mining outside the site boundary could occur at anytime until available resources are exploited. Mining activities inside the boundary should not occur until sometime after active institutional controls are no longer practicable. The types of scenarios will generally be the same regardless of the assumed location of the mining operations and will, in the main, involve events which alter the rate and volume of radionuclide movement through groundwater to the boundary of the accessible environment. It does not appear that mining can seriously impact repository performance unless boreholes, which intrude the waste panels, are also present. Without the presence of an intruding borehole, there is no obvious way to connect the waste with the overlying water-bearing formations which can then provide a lateral transport path.

The most common mining scenario assumes that subsidence of overburden into the excavated region can alter the hydraulic conductivity of the overlying water-bearing strata (e.g., the Culebra member of the Rustler Formation), possibly increasing transport velocities and/or radionuclide mass-fluxes to the accessible environment. Sandia National Laboratories (SNL) summarized the situation as follows (AXN94):

> "Although the land surface in subsiding areas is lowered and there may be local changes in drainage patterns, the overall topographic features that have the primary effect on the water table will remain similar to those of the present. However, subsidence may have impacts other than lowering of the land surface, including possible fracturing of units that overlie the potash zone. This fracturing could lead to an increase in conductivity for those units. The degree of increase and the relative change in conductivity from unit to unit could have an effect on the long-term groundwater flow behavior for Rustler units.
>
> Because the Tamarisk and Forty-niner members presently have very low conductivities, fracturing may cause larger [percentage] increases in conductivity in those units than in the Culebra and Magenta. The effect on flow would be similar to that described for boreholes that do not intrude the repository [ref. omitted] for the same fundamental reasons. That effect would be a change in the direction of the hydraulic gradients in the land withdrawal area. Currently they direct flow in the Culebra from north to south. If the scenario were to occur, they would direct flow in the Culebra towards the southwest."

Detrimental mining-related scenarios might include:

- Increased hydraulic conductivity of water-bearing formations above the mining horizons due to subsidence (Section 4)
- Change in flow directions within water-bearing members if a vertical hydraulic connection is created by subsidence (Section 5.2)
- Formation of subsidence-related surface depressions where water could accumulate and alter local recharge characteristics (Section 5.3)
- Increased hydraulic gradient if significant flow from water-bearing strata into the mine workings occurs (Section 5.4)
- Damage to borehole or shaft seals by subsidence effects (Section 5.5)
- Problems created by solution mining (Section 5.1)
- Increased hydraulic conductivity of the Salado due to excavation induced stresses (Section 5.6)

Depending on the location of the mining operations, some of these same scenarios may actually be beneficial. For example, depending on the location, flow of water into underground mine workings might also reduce the hydraulic gradient in the currently envisioned flow path. Of the potentially detrimental scenarios, the only one expected to be of greatest concern is hydraulic conductivity increases in certain strata above the mining location.

The detrimental aspects of these scenarios will be discussed in more detail subsequently, but a review of relevant technical literature will be presented first to establish a framework for that discussion.

3. Literature Review

3.1 WIPP RELATED STUDIES

3.1.1 Final Environmental Impact Statement

In the WIPP Final Environmental Impact Statement (FEIS) published in 1980, DOE summarized, without comment, prior studies on potash mine subsidence in the area as reported by the BLM in 1975 (DOE80). At that time, it was estimated that subsidence was likely to have occurred over an area of 14 square miles and was expected over an additional 40 square-mile area. The nearest subsidence to the WIPP site occurred at a distance of 3.5 miles. Observed maximum surface subsidence varied from 2.7 to 5.3 feet. This is about two-thirds the height of the mined ore zone.

3.1.2 D'Appolonia Studies

The impact on the WIPP of neighboring potash mines was examined in greater detail by D'Appolonia in 1982 (DAP82). They observed that, even when subsidence occurs, the integrity of the overlying salt section is not jeopardized as demonstrated by the absence of water flow into the potash mines from units higher in the stratigraphic section.

However, D'Appolonia noted that "the opening of entries for underground potash mining causes a redistribution of stresses within the surrounding rock that can lead to opening of fissures and/or increase the hydraulic conductivity of the surrounding rock. Mining can also lead to the more gross effects of surface subsidence and subsidence-induced fracturing above the mined level." Both empirical and simple analytical techniques were used to characterize the extent of such disturbances.

Using a secondary creep law for the salt, they calculated the zone of influence in a horizontal plane around a hypothetical potash mine (at depth of 2000 ft) and a repository room to be 1,900 and 200 feet, respectively. Thus, if the horizontal separation is 2,100 feet, there would be no stress-induced interaction between the two mined regions. D'Appolonia believes this calculation to be conservative because the WIPP also has a vertical separation from the McNutt of about 400 feet.

Estimates were also made of the impact on the hydraulic conductivity of the salt from reducing the confining stress in the salt. This occurs due to stress relief around an excavation. Based on an empirical relationship between salt permeability, octahedral shear stress, and mean confining stress, D'Appolonia calculated the increase in hydraulic conductivity to be less than one order of magnitude. At a distance into the salt of six times the width of mine opening the calculated hydraulic conductivity was only about twice the conductivity of the undisturbed salt.

D'Appolonia suggested that a generalized subsidence equation developed for coal mines in the Appalachian region could be used for making preliminary estimates of the magnitude of surface subsidence as follows:

$$S = sHbe$$

where

- S = maximum subsidence (ft)
- s = subsidence factor (dimensionless)
- H = cavity height (ft)
- e = extraction ratio (dimensionless)
- b = fraction of cavity remaining after backfill (dimensionless)

The subsidence factor is the ratio of the actual vertical displacement to cavity height which in the Carlsbad area is about 0.67. From this equation, assuming no backfill (b=1), a mining height of 6 feet, and an extraction ratio of 90%[7] the maximum subsidence would be about 3.6 feet (1.1 m).

As noted previously, potash is sometimes recovered by solution mining although this technique is not being used in the vicinity of the WIPP. According to D'Appolonia, solution mining of langbeinite is not technically feasible because the ore is less soluble than the surrounding evaporite minerals. Solution mining of sylvite was unsuccessfully attempted in the past. Failure of solution mining was attributed to low ore grade, thinness of the ore beds, and problems with heating and pumping injection water. Unavailability of water in the area would also impede implementation of this technique. For these reasons, solution mining is not currently used in the KPLA. In addition, consideration of solution mining on the

[7] According to BAR93, 60 to 75% of the ore is extracted during initial mining, but subsequent removal of the remaining pillars results in extraction ratios exceeding 90%.

disposal system in the future is excluded on regulatory grounds. According to §194.33(d), "with respect to future drilling events, performance assessments need not analyze the effects of techniques used for resource recovery subsequent to drilling of the borehole."

However, the possibility exists that solution mining could be used in the vicinity of the disposal system in the near term. As required by §194.32(c), "performance assessments shall include an analysis of the effects on the disposal system of any activities that occur in the vicinity of the disposal system prior to disposal and are expected to occur in the vicinity of the disposal system soon after disposal. Such activities shall include, but shall not be limited to, existing boreholes and the development of any existing leases that can reasonably be expected to be developed in the near future, including boreholes and leases that may be used for fluid injection activities." The chief chemist (Douglas W. Heyn for IMC Kallium (a local potash producer) provided written testimony to EPA related to the Agency's rulemaking actvities on the DOE Compliance Certification Application for WIPP. Heyn concluded that "the rational choice for extracting WIPP potash ore reserves would be by conventional room and pillar mechanical means" (HEY97).

DOE has also reviewed this issue and concluded that, even if solution mining were conducted, the principle impact would be mine subsidence which has already been accounted for in performance assessment (DOE97).

3.1.3 IT Corporation Backfill Engineering Analysis

In 1994, IT Corporation reported the results of analytical and empirical subsidence studies for the WIPP repository (ITC94). The thrust of these studies was to evaluate the effects of various backfill options on repository subsidence. The effects of potash mines in the vicinity on repository integrity were not addressed, per se. Never-the-less, some generally applicable subsidence information was developed. IT used four techniques to analyze subsidence caused by excavation of the repository:

- Mass conservation method
- Influence function method
- National Coal Board method
- Two-dimensional numerical modeling (with the Fast Lagrangian Analysis of

Continua [FLAC] computer code)

As shown in Table 3-1, reasonable agreement was obtained among the four techniques with maximum subsidence at the surface calculated to vary from 0.55 to 0.95 meters for the empty waste area.

Using the FLAC two dimensional, finite element code, the maximum vertical tensile strain in the Culebra dolomite due to projected WIPP subsidence was calculated to be 0.0034%.

Using the influence function method,[8] ITC developed contour plots showing the areal extent of surface subsidence caused by repository excavation. The limit of subsidence area was about 850 feet beyond the southern edge of the repository footprint. From this analysis, ITC concluded that, since the maximum subsidence was about 0.4 m and since local surface topography varied by more than 3 meters, a subsidence basin would not be created and repository subsidence should not be visible.

[8] The influence function method assumes that each point in an excavation has an identical circular area of influence on surface subsidence. These influence areas are superimposed to obtain the cumulative effect of all extraction elements.

Table 3-1. Summary of IT Corp. Subsidence Prediction Results for WIPP Repository (ITC94)

Underground Area	Contents of Excavation	Subsidence				
		Mass Conservation (m)	Influence Function Method (m)	NCB Method (m)	FLAC Single-Room Model (m)	FLAC Full-Panel Model (m)
Waste Emplacement Area[a]	Empty	0.86	0.56	0.73	0.95	0.55
	Waste Only	0.62	0.40	0.53	NA	NA
	Waste plus loose backfill	0.55	0.36	0.47	0.33	NA
	Waste plus compacted backfill	0.52	0.34	0.44	0.30	NA
Shaft Pillar Area	Empty	0.28	0.10	0.04	NA	0.13[b]
	Loose backfill	0.12	0.04	0.02	NA	NA
	Compacted backfill	0.06	0.02	0.01	NA	NA
Northern Experimental Area	Empty	0.24	0.08	0.02	NA	NA
	Loose backfill	0.11	0.04	0.01	NA	NA
	Compacted backfill	0.05	0.02	0.01	NA	NA

[a] Waste emplacement area includes Panels 1 through 8; 2 through 8 are not yet excavated.
[b] At the Waste Shaft
NCB National Coal Board
FLAC Fast Lagrangian Analysis of Continua .
NA Not Available.
m Meters.

3.1.4 SNL Studies of Subsidence

SNL has explored the possible impact of WIPP subsidence on PA. In a 1989 study to select events and processes which should be considered in forming possible scenarios, SNL considered three possible processes related to repository-induced subsidence (HUN89):

- Increased hydraulic conductivity of the Salado Formation
- Fracturing
- Disruption of surface drainage

Based on the fact that repository excavation would produce a maximum of a 0.2% increase in the volume of the overlying Salado salt, they concluded that increased Salado hydraulic conductivity would be insignificant. They further concluded that fracturing of the Salado could also be neglected. This conclusion was based on the expectation that the repository would adjust to excavation by creep rather than fracturing. This position was supported by observations in local potash mines where mining was conducted with two levels of extraction. The observed response of the rock in the upper horizons was flexure rather than fracture. However, SNL stated that effects on the Culebra were unknown. With regard to surface drainage, SNL concluded that this would not be a factor because, with a maximum expected surface subsidence of 2 feet, there was no integrated drainage which would be disrupted.

As noted in Section 2 above, SNL revisited the subsidence issue in 1994 concluding that subsidence could cause fracturing in the more brittle overlying units which could result in increased hydraulic conductivity and possible redirection of flow in the Culebra from a generally north to south direction to a more southwesterly direction (AXN94). Surface subsidence effects were not expected to be of sufficient magnitude to significantly alter the position of the water table.

3.2 OTHER RELEVANT STUDIES

3.2.1 New Mexico Potash Mines

IT Corporation summarized subsidence observations made at potash mines in southeastern New Mexico (ITC94). Observed angles of draw, measured from vertical edge of the mine workings to the point where surface subsidence ceased, varied from 25 to 58 degrees. ITC noted that the maximum observed subsidence over four potash mines in the area varied from

0.4 to 1.5 m which was between 16 to 66% of an assumed excavation height of 2.6 m (8.5 ft)[9]. ITC felt that the maximum observed subsidence was less than that which will ultimately occur over the excavated area.

3.2.2 Coal Mines

A large body of subsidence literature has been developed based on coal mining in the United States and the United Kingdom. In a number of studies, subsidence-induced increases in transmissivity are described. Some examples are provided here.

The U.S. Geological Survey described the effects of subsidence associated with longwall mining of coal in Marshall County, West Virginia (USG88). Three tests were recounted where the transmissivity of a perched aquifer was measured before and after mining a coal seam. In each case, the overburden was about 800 feet thick and the tested aquifer was between 25 and 150 feet below the surface. In two tests, the transmissivity was found to increase significantly, from 3.7 to 160 ft^2/day in one case and from less than 0.001 to 36 ft^2/day in the other. In the third test, only a slight increase between pre- and post-mining transmissivity was observed (from 0.20 to 0.31 ft^2/day). This small change was attributed to the fact that significant subsidence fracturing had not occurred.

Booth discussed to similar studies related to longwall coal mining in the Illinois Basin (BOO92). One series of tests was conducted at a site in Jefferson County, Illinois where coal seams 9 to 10 feet thick were mined at a depth of about 725 feet. The overburden consisted primarily of low permeability shales, siltstones and limestones. An aquifer in sandstone exists about 75 feet below the surface which is confined by an overlying shale unit. Subsidence produced visible surface tension cracks. Subsurface strain measurements and borehole examination indicated fractures and bedding plane separation. In three pre-subsidence measurements, made during pumping the same well for three increasing time periods, values of hydraulic conductivity in the Mt. Carmel sandstone were 2×10^{-6}, 2×10^{-5}, and 3×10^{-6} cm/s. After subsidence, measured values were 5×10^{-5}, 3×10^{-5}, and 4×10^{-5} cm/s for similar pumping periods. In another paper discussing the same site, it was reported that post-subsidence values of the hydraulic conductivity in the shale were increased by two

[9] The maximum observation period varied from one week to more than one year.

to three orders of magnitude (KEL91).

At a second site in Saline County, IL, investigations involved subsidence related to mining a five- to six-foot coal seam at a depth of about 400 feet (BOO92). The Trivoli sandstone aquifer lies above the seam and about 180 feet below the surface. Initial conductivities in the Trivoli were less than 10^{-8} cm/s and these increased to about 5 x 10^{-6} cm/s after mining. Booth attributed this increased conductivity to the supposition "that subsidence had probably improved the interconnectedness of permeable fractures."

The U.S. Bureau of Mines described hydrologic changes associated with longwall mining of coal in Cambria County, Pennsylvania (MAT92). The coal seams studied were at a depth of 740 to 845 feet and were overlain by fine-grained sedimentary rocks and thin coal beds. Only small changes in hydraulic conductivity of the overburden due to mining were measured. Increases were a factor of 2 to 4 and in some cases an unexplainable decrease were noted. The increased conductivity was attributed to excavation-induced creation of new passages for groundwater flow.

Elsworth and Liu used non-linear finite element modeling to estimate changes in hydraulic conductivity associated with longwall mining (ELS95). In their modeling, a 140-foot thick zone of increased horizontal conductivity caused by vertical strains was defined immediately above a 5-foot thick coal seam. The estimated conductivity increase was about an order of magnitude.

Bai and Elsworth described modeling studies involving the interrelationship between subsidence and stress dependent hydraulic conductivity (BAI94). In concept, the rock mechanics approach was similar to that taken in this study and described in Section 4 below. In the Bai and Elsworth studies, finite element analyses over representative stratigraphy were used to calculate changes in hydraulic conductivity for various fracture spacings.

4. Impact of Mining on Hydraulic Conductivity

4.1 BACKGROUND INFORMATION

Based on the available site information, it appears that one of the potential detrimental results of mining near the repository could be increased hydraulic conductivity[10] of the brittle water-bearing strata above the mining horizons. In the analysis presented here, the focus is on the Culebra Member of the Rustler Formation which is the most transmissive unit. The Culebra can potentially provide a lateral conduit to the accessible environment if contamination from the repository 1440 feet below reaches the transmissive horizon. According to SNL, the Culebra is a "finely crystalline, locally argillaceous (containing clay) and arenaceous (containing sand), vuggy dolomite ranging in thickness near the WIPP from about 7 m (23 ft) .... to 14 m (46 ft) ....." (Docket: A-93-02, Ref. #563). In its 1992 PA, SNL chose 7.7 meters as the reference thickness. However, for the CCA the DOE reduced this thickness to 4.0 m. Using information from 41 boreholes, SNL has calculated that the transmissivity of the Culebra varies by about six orders of magnitude depending on the degree of fracturing which exists (SAN92). Since transmissivity is a field measured value the assumed reduction in effective thickness, for the CCA, will have no impact on either the groundwater, flow analysis, or the transmissivity values used. In the 1992 PA (SAN92), the median fracture spacing was assumed to be 0.4 m and range between 0.062 and 8 m. Thus, the median number of horizontal fractures through the Culebra thickness would be 19 and the range would lie between 1 and 124. Based on recent work investigating the Culebra hydrogeology as described in Holt (1997) the assumption of 1 fracture would be highly conservative and unrealistic.

If subsidence occurs, it may create a network of both vertical and horizontal strains in the Culebra. Vertical tensile strains can increase the aperture of existing horizontal fractures; whereas, horizontal tensile strains can increase the aperture of existing vertical fractures. Compressive strains would have the opposite effect. An increase in fracture aperture results in an increase in hydraulic conductivity. This increased hydraulic conductivity can reduce lateral travel time of radionuclides to the accessible environment at the vertical subsurface extension of the site boundary.
In light of the 1992 PA and CCA assumption that Culebra flow and transport are through

[10] The terms hydraulic conductivity and transmissivity are sometimes used interchangeably in the text as indicators of altered flow path resistance. Transmissivity is the product of the hydraulic conductivity and aquifer thickness. In the examples presented here, the Culebra thickness is assumed to be constant so the transmissivity is a constant factor of 7.7 higher than the hydraulic conductivity (in metric units).

fractures, the discussion here focuses on one potential theory describing groundwater flow through fractures. The subsequent section (i.e., 4.2) describes how the fracture aperture increases were estimated using a two dimensional finite element analysis of subsidence-induced strains and the final section in this chapter uses the theory and the strain analysis to estimate travel times to the accessible environment.

Darcy's Law relates the movement of water in a porous medium to the hydraulic gradient and the hydraulic conductivity. The hydraulic conductivity is a measure of the transmissive capacity of the medium coupled with the density and viscosity of the fluid (water in this case). The hydraulic gradient is simply the slope of the water table (unconfined aquifers) or the potentiometric surface for a confined system. The equation for Darcy's law is

where q is the Darcy velocity (m/yr), K is the hydraulic conductivity (m/yr) and dh/dl is the hydraulic gradient (dimensionless - m/m). Hydraulic conductivity is actually a property of both the physical media (the aquifer) and the fluid. Darcy's law may also be written using intrinsic permeability (k) which is a property of the medium alone, as shown below:

where:

k = intrinsic permeability (m^2)
ρ = fluid density (kg/m^3)
μ = viscosity ($Pa \cdot s$)
g = gravitational constant (m/s^2)

The advective flow rate for a conservative contaminant (i.e., non-sorbing and nonreactive) migrating through a porous medium is computed by dividing the Darcy velocity (given above), by the effective porosity. The effective porosity for a porous medium is the ratio of the connected void space divided by the total volume of the medium.

In a fractured medium, Darcy's law still applies, however, the hydraulic conductivity of the fracture (K_f) is more difficult to determine. If the fractures are conceptualized as a series of parallel plates (with the fractures being the gaps between adjacent plates), mathematical equations can be derived to determine the equivalent hydraulic conductivity that would be

used in Darcy's law.

The porosity of the fracture system actually should be viewed as two components, fracture porosity and matrix porosity. Using the parallel plate analogy, the fracture porosity is the number of fractures times the fracture aperture (gap thickness) divided by the thickness of the aquifer. The matrix porosity is the porosity of the blocks of rock between the fractures. In a fractured system such as granitic rock, the matrix porosity may be effectively zero because there is no intergranular void space. However, there is some measurable porosity space within the Culebra matrix (Docket: A-93-02, REf. #563).

The hydraulic conductivity of a system of horizontal fractures is determined by the fracture aperture and the spacing between fractures. Given an equivalent hydraulic conductivity of the aquifer (i.e., determined through aquifer testing) and fracture spacing, it is possible to compute the fracture hydraulic conductivity. The calculation is based upon moving the same flux of groundwater through the fracture system as through a porous medium. The derivation of this equation is developed below.

The fracture conductivity equation is derived in two steps. First, the hydraulic conductivity for a single fracture is defined and then this is related to the flow rate through the fracture. The hydraulic conductivity of a single fracture is given as:

(1)

where:

b = half-fracture aperture (m)

K_f = fracture hydraulic conductivity (m/yr)

This equation is presented in a number of papers such as Snow (SNO69) and Gale (GAL82). The equation is often rewritten in terms of the full fracture aperture, as follows:

(2)

where:

w = full fracture aperture ($b^2 = w^2/4$) (m)

The second step in computing the aperture from an equivalent porous medium K value is to equate the flow rates through the porous and fractured systems. The flow through a set of N horizontal fractures of identical aperture is:

(3)

where:

Q_f = flow rate through the fractures (m^3/yr)
L = length of fractures perpendicular to flow (m)
N = number of fractures

The term (NwL) is the area term in a traditional Darcy's law equation. The equation for flow through an equivalent porous medium would be:

(4)

where:

K_ϵ = equivalent porous medium hydraulic conductivity (m/yr)
D = aquifer thickness (m)
L = length perpendicular to flow direction (m)

As mentioned above, equation 4 may also be written in terms of intrinsic permeability (k) and fluid properties, as show below:

(4b)

To compute an equivalent K for the porous medium, the flow rates through the two systems (porous and fractured) must be equal. Setting equation 3 equal to equation 4 yields:

(5)

with common terms canceling from the equations. This equation can then be rearranged to give an equation of fracture aperture in terms of an equivalent porous medium hydraulic conductivity:

(6)

Finally, to transform the equation into terms of spacing between fractures ($D_f = D/N$), the equation becomes:

(7)

After computing the fracture aperture for a given porous medium hydraulic conductivity (equation 7), the fracture hydraulic conductivity is computed from equation 2 above. It can be seen from equation 2 that the fracture hydraulic conductivity (K_f) varies as the square of

the aperture (w) while the equivalent porous medium conductivity (K_ϵ) varies as the cube of the aperture.

The following example provides an indication of the magnitude of changes which might be expected in the Culebra hydraulic conductivity resulting from subsidence induced fractures. For these calculations, it is assumed that the vertical tensile strain produced by subsidence results in the opening of existing horizontal fractures rather than the creation of new fractures. The total strain is accommodated by increasing the fracture aperture. Thus, if, for discussion purposes, there is a single horizontal fracture in the Culebra and subsidence from potash mining causes 0.03% vertical tensile strain (which is about 10 times the value calculated in ITC94 for the Culebra from repository subsidence, see Section 3.1.3 above), the total displacement is 2.3×10^{-3} m (7.7 m x 0.0003). If 10 horizontal fractures were present, then the increase in each aperture would be 2.3×10^{-4} m.

The effect of subsidence on changes in fracture aperture and hydraulic conductivity of the Culebra for the case of 10 fractures across the aquifer thickness is calculated using the following assumptions:

aquifer thickness (D)	= 7.7m
viscosity(μ)	= 0.001 Pa•s
density (ρ)	= 1000 Kg/m^3
gravitational constant (g)	= 9.79 m/s^2
equivalent hydraulic conductivity (K_ϵ)	= 7.0 m/y = 2.24×10^{-7} m/s
tensile strain	= 0.03% = 0.0003 m/m
total displacement	= 7.7m x 0.0003 strain = 2.3×10^{-3}m

The attendant fracture aperture from equation (6) is:

(8)

K_ϵ = equivalent hydraulic conductivity
w = fracture aperture
ρ = density
g = gravitational constant
N = number of fractures
μ = viscosity
D = aquifer thickness

$$w = 5.96 \times 10^{-5} \text{ m}$$

For a total displacement of 2.3 x 10^{-3} m, the displacement per fracture is 2.3 x 10^{-4} m and the expanded fracture aperture resulting from the tensile strain (w_{strain}) is

$$w_{strain} = 5.96 \, x \, 10^{-5} + 2.3 \, x \, 10^{-4} = 2.9 \, x \, 10^{-4} \text{ m}$$

To calculate the strain-altered equivalent hydraulic conductivity, $K_{\epsilon s}$,

(9)

Values of the equivalent hydraulic conductivity for various assumed values of N within the range used in the 1992 PA are summarized below based on 0.03% vertical tensile strain:

N (fractures)	K_{es}, Hydraulic Conductivity (m/y)
1	4.8 x 10^{4}
10	8.2 x 10^{2}
100	4.4 x 10^{1}

From this hypothetical example, it can be seem that the strain-induced change in hydraulic conductivity (from a base of 7 m/g) is nearly four orders of magnitude for a single fracture and only a factor of six for 100 horizontal fractures through the thickness of the Culebra. Furthermore, DOE's assumption that the effective thickness or the Culebra is 4.0m would lead to hydraulic conductivities that are approximately 60% higher for the 10 fracture scenario. However, it should be kept in mind that DOE reduced the thickness of the Culebra because ground-water flow was only occuring in the lower portion of the unit. From a structural unloading standpoint the entire Culebra thickness of 8m is available to dissipate the stress. Therefore, 8m is a more realistic value in estimating stress related changes to the Culebra.

In order to provide a more detailed view of the impact of subsidence on repository performance, a series of modeling simulations were made. First, the strain distribution in the Culebra Dolomite as a function of distance from the face of a potash mine was calculated using a two-dimensional finite element model (the UTAH2 computer code). Then, this strain distribution was assumed to be accommodated as increases in the aperture of existing fractures. Details of these analyses are presented in subsequent sections.

4.2 STRAIN ANALYSIS

A preliminary analysis was conducted to estimate the effects of simulated mining of potash near the WIPP site on the hydraulic conductivity of the Culebra Member of the Rustler Formation. Simulation of longwall mining of potash was done using a two-dimensional finite element computer program, UTAH2. This program has been in use for many years and is considered quite reliable (PAR78, PAR91). In response to mining, the adjacent rock mass moves to a new equilibrium position. Maximum surface subsidence occurs above the center of a mined panel, but diminishes with distance from the panel center. However, as will be shown, maximum strains do not occur at the same location as maximum subsidence. Tensile strains may open existing joints or fractures and fracture opening is assumed to increase hydraulic conductivity. If tensile strain between existing fractures is assumed to be absorbed entirely by fractures, then the change in fracture aperture can be calculated. With the assumption of an initial aperture, the change in hydraulic conductivity can then be estimated as shown in Section 4.1.

4.2.1 Finite Element Analysis

The UTAH2 finite element program is a small strain, elastic-plastic computer program that uses associated flow rules in conjunction with a pressure-dependent yield criterion. Elastic and strength anisotropy may be independently specified, but one material axis is tacitly assumed to be normal to the plane of analysis. The form of the yield criterion is $J_2+I_1=1$, where J_2 is an anisotropic form of the second invariant of deviatoric stress and I_1 is an anisotropic form of the first invariant of stress. The isotropic form is a paraboloid of revolution about the hydrostatic axis in principal stress space. Essential input data include the elastic moduli as well as the strength parameters, geologic column, mining geometry, boundary conditions and the premining stress state.

4.2.1.1 Material Properties

For the isotropic case analyzed here, the strength parameters required are the unconfined compressive (C_o) and tensile (T_o) strengths of each material represented in the finite element mesh. The elastic parameters are Young's modulus (E) and Poisson's ratio (ν) for each material. Specific weights (γ) of the various rock types present in the model region are also needed. The data for the four rock types assumed in the model are given in Table 4-1.

Sandstone, anhydrite and halite elastic properties were obtained from a subsidence analysis of the WIPP repository conducted by the IT Corporation (ITC94). Strengths, with the exception of halite were also obtained from (ITC94). Dolomite properties and halite strength are averages of about 20 results obtained from a standard handbook (LAM78).

Table 4-1. Rock Properties By Type

Rock Type	E(10^6 psi)	ν	C_o(10^3 psi)	T_o(10^3 psi)	γ (pcf)
Sandstone	3.8	0.21	15.0	5.0	144
Anhydrite	10.9	0.35	13.3	4.6	144
Dolomite	9.4	0.30	13.3	1.2	144
Halite	4.5	0.25	5.2	3.1	144

Consideration of strength and elastic modulus properties for the Culebra shows that the strain at failure under uniaxial compression is 0.14%. Under tension the strain at failure is 0.013%. Rock strength is strongly affected by confining stress, so under multiaxial compressive stress, the strain at failure should be greater than in the uniaxial case. Tensile strength is not considered sensitive to confining stress, so tensile strain at failure would also be insensitive to confining stress. These estimates of failure strain are based on the laboratory test data summarized in Table 4-1. The rock mass would have different properties depending on fractures that are present in the field, but absent in the laboratory test samples. Strains calculated using laboratory data will be lower than strains calculated using field-scale properties.

4.2.1.2 Geologic Column

The geologic column used in the analysis was adapted from the ERDA 9 borehole near the center of the WIPP site (POW78). Table 4-2 gives the depth, formation, and thickness of the different strata represented in the finite element model.

Table 4-2. Strata Depth and Thickness at WIPP Site

Formation	Depth (ft)	Thickness (ft)
1. Dewey Lake	0	550
2. Rustler	550	58
3. Magenta	608	24
4. Rustler	632	82
5. Culebra	714	26
6. Rustler	740	120
7. Upper Salado	860	507
8. McNutt	1,367	176
9. Potash Seam	1,543	10
10. McNutt	1,553	188
11. Lower Salado	1,741	333
12. Storage Zone	2,074	104
13. Lower Salado	2,178	442
14. Storage Zone*	2,620	110
15. Lower Salado	2,730	106
16. Castile	2,836	1,664[11]

* Not included in analysis, Salado properties assumed.

As can be seen from Table 4-2, the base of the mesh includes a portion of the Castile Formation to a depth of 4,500 ft (2836+1664). All strata below the Rustler Formation were assigned halite properties from Table 4-1. The Rustler Formation was assigned anhydrite properties (except for the Culebra and Magenta members which were assigned dolomite properties). The Dewey Lake Formation was assigned sandstone properties. These assignments of properties are the same as used in ITC94.

[11] The thickness assigned to the Castile does not include the entire unit, rather it is based on assumptions regarding the necessary modeling depth required to minimize boundary effects.

4.2.1.3 Mining Geometry

The mining panel was assumed to be 10 ft thick[12], 3,000 ft long and located near the middle of the McNutt. However, the center of the panel is assumed to be a line of symmetry, so only 1,500 ft is explicitly represented in the mesh. As a rule of thumb, the influence of an excavation extends "one diameter" from the excavation walls. At one diameter, the stress concentration about a circular hole decreases to within about 15% of the initial stress state. The "diameter" that characterizes non-circular holes is the long dimension of the hole. In this case, the "1-D" guideline suggests that panel excavation may noticeably influence the state of stress 3,000 ft away. Thus, about 3,000 ft was added to the panel depth (1,543 ft) to obtain a vertical mesh dimension of 4,500 ft. The horizontal dimension of the mesh extends 5,250 ft beyond the panel edge and is thus 6,750 ft. The mesh and panel are shown in Figures 4-1 and 4-2 where the scale is 900 ft per inch. There are 4,050 elements and 4,216 nodes in the mesh. The element aspect ratio is 5 or less.

4.2.1.4 Premining Stress State

The premining stress state was attributed to gravity alone; no tectonic stresses were assumed. The vertical stress is then simply the average unit weight of rock times depth. Under complete lateral restraint, the horizontal premining stress is a constant, K_o, times the vertical stress. The constant depends on Poisson's ratio, ν, and is therefore different for each rock type. In fact, $K_o = \nu/(1-\nu)$, which ranges from about 0.2 to 0.5 based on the values in Table 4-1.

4.2.1.5 Boundary Conditions

The centerline of a panel was a line of symmetry; no displacement was allowed normal to this line. Zero displacement boundary conditions were also specified normal to the mesh bottom and far side. A zero normal displacement is often represented by a roller. The top of the mesh coincided with the ground surface and was unrestricted except at the sides.

---

[12] This thickness was selected as a conservative value based on mine workings in the area (Section 3.2.1) and to reflect the possibility of mining on multiple levels.

Displacement boundary conditions were also specified on the excavation surface. The panel roof was specified to "sag" 9 inches per load step; the floor was specified to "heave" 3 inches per load step. Thus, 1 foot of closure occurred during each load step at every pair of nodes along the panel except at the panel edge where traction boundary conditions, equal but opposite in sense to the premining stresses, were applied. The amount of seam level closure is controlled by the number of load steps specified, but is physically limited to a maximum of 100% of the mined thickness (10ft).

Figure 4-1. Finite Element Mesh Used for Strain Analysis Mesh 4,500 ft by 6,750 ft.

Figure 4-2. Half Width (1,500 ft) of Mined Panel.

A second physical constraint on seam closure is the amount of subsidence observed at the surface. The number of load steps was adjusted to meet these constraints. Specifically, seam level closure (relative displacement between roof and floor) is 70% when 7 load steps are applied. The corresponding surface subsidence calculated at the panel centerline is 52.5% of the seam thickness. When 9 load steps are applied, seam level closure is 90%, while surface subsidence is 67.5% of seam thickness. This range of surface subsidence is considered reasonable for full-extraction potash mining.

4.2.2 Fracture Conductivity Change

As described above in Section 4.1, the parallel plate model for fracture flow states that average flow velocity is proportional to the square of the thickness (aperture) of the fracture; the volume flow rate (discharge) is proportional to the cube of the aperture (equation 3). Fracture hydraulic conductivity, K_f, is used here to relate flow velocity to hydraulic gradient and is thus proportional to the square of fracture aperture (equation 2). The relative change in hydraulic conductivity is $(K_f - K_{fo})/K_{fo}$ where K_{fo} is the premining fracture hydraulic conductivity. A purely geometrical calculation gives the relative change. Thus, the relative change in fracture hydraulic conductivity is $(w^2-w_o^2)/w_o^2$, where w is the fracture aperture after mining (i.e. w_{strain}) and w_o is premining fracture aperture. This ratio is independent of the units used for hydraulic conductivity such as feet or meters per year.

The post-mining aperture is simply the premining aperture plus the change in aperture, Δw, induced by mining. This change is the strain, ϵ, integrated over fracture spacing, D_f, that is, $\Delta w = D_f \epsilon$. Fracture spacing was assumed to vary between 3 and 300 inches (ca. 0.08 m and 8 m); initial aperture was assumed to vary from 10^{-4} to 10^{-2} inches.[13] Strains are obtained from the finite element simulation of longwall potash mining.

[13] In metric units these apertures are equivalent to 2.5 x 10^{-6} to 2.5 x 10^{-4} m. This range of apertures would be associated with equivalent hydraulic conductivities varying from about 6 m/y to about 60,000 m/y. In SAN92, reported hydraulic conductivities (converted from transmissivities using an aquifer thickness of 7.7 m) within the WIPP Land Withdrawal Area ranged from 0.026 to 4,400 m/y.

4.2.3 Strain Analysis Results

Two simulations were preferred. The first was associated with a subsidence factor (S) of 52.5% (maximum surface subsidence as a percentage of mined panel height); the second was associated with a subsidence factor of 67.5%. The results are similar in trend, but differ quantitatively.

4.2.3.1 Case 1 (Substance Factor of 52.5%).

Horizontal and vertical strains in the Culebra member of the Rustler Formation are shown in Figure 4-3 for this case (S = 52.5%). The data are strains which are calculated at the centroid of the model elements in the Culebra. Tensile strain is positive in Figure 4-3. The horizontal axis begins at the left edge of the finite element mesh, that is, at the center of the mined panel. Mining extends 3,000 ft, but taking advantage of the symmetrical nature of the problem only, 1,500 ft needs to be incorporated into the mesh. Figure 4-3 shows tensile strain in the vertical direction over the mined panel (between 0 and 1500 ft) and horizontal tensile strain beyond the edge of the panel (beyond 1500 ft). The peak vertical tension (E-V) is about 0.055% (550 micro-in./in) and occurs 1,075 ft from the panel center (i.e., 425 ft inside the panel edge). The peak horizontal tensile strain (E-H) occurs 175 ft outside the panel edge and is 0.0085% (85 micro-in/in). The horizontal tensile strain initially decreases with distance from this peak and then rises to a broad secondary maximum of about 0.0047% (47 micro-in/in) at 4,275 ft from the panel center after which it decays slowly with increasing distance.

The horizontal strain changes from tension outside the mined panel to compression inside as seen in Figure 4-3. The peak horizontal compression occurs inside the panel and gradually decreases to a minimum at the panel center where the slope of the plot is zero. This trend is indicative of a panel that is sufficiently wide relative to depth to cause maximum subsidence.

The panel has super-critical width in subsidence terminology. Critical width is usually given in terms of the angle of draw(s): $W_c = (2H)\tan(\delta)$. If the angle of draw is 35^o, e.g., then critical width is 1.4H where H is the overburden thickness.

Vertical tensile strains would tend to open horizontal fractures, while horizontal tensile

strains would tend to open vertical fractures. Compressive strains would tend to close fractures. The

Figure 4-3. Subsidence-induced Culebra strains for subsidence factor of 52.5%. (Panel extends +/-1,500 ft from origin)

magnitude of the vertical tensile strain near the center of the mining panel is about the same as the horizontal compressive strain outside the mining panel and away from the rib. So the change in hydraulic conductivity of horizontal joints over the panel is about the same as the change in vertical joint conductivity for a substantial distance outside the mining panel (neglecting peaks near the rib).

Figure 4-4 shows the change in *vertical* fracture apertures (opening or closing) in the Culebra as a function of distance from the panel center for three assumed joint spacings (3, 30 and 300 inches or approximately 100, 10, and 1 fractures through the thickness of the Culebra). Because vertical fractures or joints respond to horizontal strain, joint closure occurs over the mined panel where the horizontal strain is compressive. Vertical joints tend to open outside the mined panel. The magnitude of aperture change increases significantly with joint spacing. Vertical joint opening which occurs outside the mined panel ranges from nil to almost 0.03 inches near the rib.

Figure 4-5 shows the aperture change for horizontal joints (which respond to vertical strain). The peak aperture changes at a 300-inch joint spacing are cut off in the plot. Horizontal joint opening which occurs above the mined panel ranges from nil to well over 0.04 inches.

Negative aperture changes 0.06 inches or greater are indicated in Figures 4-4 and 4-5. Aperture closures of this magnitude are not physically possible in most cases since apertures are likely to be $\leq 10^{-2}$ (see 4.2.2). The excess compressive strain would be absorbed elastically by the rock mass. Additional fractures would not result since the compressive fracture strain of -0.14% is not exceeded (see 4.2.1.1).

Figure 4-6a is a semilog plot of the relative increase in hydraulic conductivity of vertical fractures, spaced 3 inches apart, that is induced by horizontal tensile strain outside the mined panel. The relative change depends on the initial fracture aperture; 3 apertures ranging from 10^{-4} to 10^{-2} inches are assumed in the construction of Figure 4-6a. Only fractional increases occur below the x-axis in Figure 4-6a (i.e., changes are less than an order of magnitude), while orders of magnitude increase are shown above the x-axis. Figures 4-6b and 4-6c present similar results at joint spacings of 30 and 300 inches. Generally, the relative increase is greater for smaller, more widely spaced joints or fractures.

Figure 4-4. Aperture Change in Vertical Joints for Fracture Spacings of 3, 30, and 300 inches and Subsidence Factor of 52.5%

Figure 4-5. Aperture Change in Horizontal Joints for Fracture Spacings of 3, 30, and 300 inches and a Subsidence Factor of 52.5%

Figure 4-6. Relative Change in Fracture Hydraulic Conductivity for Vertical Joints with Various Fracture Spacings, Subsidence Factor of 52.5%, and Fracture Apertures of 10^{-4}, 10^{-3}, and 10^{-2} in. a) 3-inch b) 30-inch c) 300-inch Spacing.

Figure 4-7. Relative Change in Fracture Hydraulic Conductivity for Horizontal Joints with Various Fracture Spacings, Subsidence Factor of 52.5%, and Fracture Apertures of 10^{-4}, 10^{-3}, and 10^{-2} in. a) 3-inch b) 30-inch c) 300-inch Spacing.

Figures 4-7a, b, and c show the relative increase in hydraulic conductivity of horizontal joints over the mined panel. Joint spacings of 3, 30 and 300 inches were used for Figures 4-7a, b and c, respectively.

4.2.3.2 Case 2 (Subsidence Factor of 67.5%).

Horizontal and vertical strains in the Culebra are shown in Figure 4-8 for this case (S = 67.5%). The peak vertical tension is about 0.071% (710 micro-in/in) and occurs inside the panel as seen in this figure. The peak horizontal tensile strain is about 0.0053% (53 micro-in/in) and occurs 225 feet beyond the panel edge. With distance, the horizontal strain becomes compressive, then reverses to tensile, and reaches a secondary maximum of 0.0053% (53 micro-in/in) at 4,375 ft from the panel center. A gradual decrease occurs thereafter. The trends in vertical and horizontal strain are similar to Case 1. However, increasing the subsidence factor increases the peak vertical tension over the mined panel but decreases the peak horizontal tension outside the mined region. The secondary peaks outside the mined region changed very little.

Vertical tensile strains shown in Figure 4-3 and 4-8 exceed the expected tensile fracture strain of 0.013% (see 4.2.1.1). Thus, as mining proceeds, fracturing in the Culebra will occur above the mined out area. These figures illustrate the strain distribution at a particular point in time when the panel width is 1,500 ft. At earlier times the rock above the panel which shows a residual strain of about 0.005% in Figures 4-3 and 4-8, would have been subjected to substantially higher strains exceeding the fracture strain.

Since the horizontal tensile strain did not decay with distance as much as expected (see Figure 4-8), the strain analysis was repeated with a larger mesh 9,000 ft by 13,500 ft. As shown in Figure 4-9, with the larger mesh, the horizontal tensile strain decayed to 7 micro-in/in at 7,025 feet from the panel center.

Figure 4-10 shows the change in *vertical* fracture aperture (opening or closing) in the Culebra formation as a function of distance from the panel center for three assumed joint spacings (3, 30 and 300 inches). Vertical joint opening which occurs outside the mined panel ranges from nil to about 0.015 inches which is a smaller range than in Case 1 because of the smaller peak horizontal tensile strain.

Figure 4-8. Subsidence-induced Culebra Strains for Subsidence Factor of 67.5% (Panel extends +/-1,500 ft from origin)

Figure 4-9. Subsidence-induced Culebra Strains for Subsidence Factor of 67.5%. (Panel extends +/-1,500 ft from origin.) Horizontal Mesh Extended to 13,500 ft.

Figure 4-10. Aperture Change in Vertical Joints for Fracture Spacings of 3, 30, and 300 inches and Subsidence Factor of 67.5%

Figure 4-11. Aperture Change in Horizontal Joints for Fracture Spacings of 3, 30, and 300 inches and a Subsidence Factor of 67.5%

Figure 4-11 shows the results for *horizontal* joints which respond to vertical strain. The peak aperture changes at a 300 inch joint spacing are cut off in the plot. Horizontal joint opening which occurs above the mined panel ranges from nil to well over 0.04 inches.

Comparison with Case 1, at a 30 inch joint spacing, shows greater horizontal joint opening in this case (somewhat more than 0.02 inches compared with somewhat less than 0.02 inches in Case 1).

Figure 4-12a shows the relative increase in hydraulic conductivity of vertical fractures, spaced 3 inches apart, that is induced by horizontal tensile strain outside the mined panel. The gap in the plot occurs as the horizontal strain outside the panel changes from tension to compression and then back to tension with distance from the panel edge. The magnitudes of the relative change in hydraulic conductivity of the joints are similar to the previous case. Figures 4-12b and 4-12c present similar results at joint spacings of 30 and 300 inches, respectively. As before, the relative increase is greater for smaller, more widely spaced joints or fractures. Relative fracture conductivity changes for horizontal joints are included in Figures 4-13a, b, and c.

As noted previously, the fracture spacings of 3, 30, and 300 inches are approximately equivalent to 0.08, 0.8, and 8 m which is comparable to the range of fracture spacings assumed in the 1992 PA of 0.06 to 8 m with a median value of 0.4 m.[14] Based on an assumed thickness of the Culebra Dolomite of 7.7 m, the number of fractures equivalent to 3, 30 and 300 inch spacings is 100, 10, and 1 respectively. The assumption of a single fracture is not realistic based on available information about the Culebra dolomite (Holt, 1997). It is included here as a conservative boundary assumption. From equation 7 in Section 4.1, the fracture apertures associated with these numbers of fractures for an equivalent porous medium hydraulic conductivity of 7 m/y are:

Spacing	N	w
300	1	5.1×10^{-3} in
30	10	2.4×10^{-3} in
3	100	1.1×10^{-3} in

[14] The Draft Compliance Certification Application (DOE95) assumed Culebra fracture spacings ranging from 0.1 to 4 m with a medium value of 0.505 m.

Figure 4-12. Relative Change in Fracture Hydraulic Conductivity for Vertical Joints with Various Fracture Spacings, Subsidence Factor of 67.5%, and Fracture Apertures of 10^{-4},10^{-3}, and 10^{-2} in. a) 3-inch b) 30-inch c) 300-inch Spacings.

Figure 4-13. Relative Change in Fracture Hydraulic Conductivity for Horizontal Joints with Various Fracture Spacings, Subsidence Factor of 67.5%, and Fracture Apertures of 10^{-4},10^{-3}, and 10^{-2} in. a) 3-inch b) 30-inch c) 300-inch Spacings.

From Figure 4-13a, it can be seen that the fracture conductivity change associated a 3-inch spacing (N=100) and a fracture aperture of 1.1 x 10^{-3}in is less than a factor of 10. Similarly, from Figure 4-13b, it can be seen that the fracture conductivity change for a 30-inch spacing (N=10) and a fracture aperture 2.4 x 10^{-3}in is less than three orders of magnitude. Finally, from Figure 4-13c, it can be seen that the fracture conductivity change for a 300-inch spacing (N=1) and a fracture aperture of 5.1 x 10^{-3}in is about 10^{5}.

As the equivalent porous medium hydraulic conductivity increases, the initial fracture aperture increases which in turn lessens the change in fracture conductivity due to subsidence. For example, if the equivalent porous medium hydraulic conductivity was 300 m/y, the initial fracture aperture would be 1.8 x 10^{-2} in and the change in fracture conductivity for a 300-inch spacing from Figure 4-13c would be less than three orders of magnitude. From this analysis, it appears that an assumed increase in hydraulic conductivity due to subsidence of three orders of magnitude is reasonable based on the median values of fracture spacing used in the 1992 PA.

4.3 FLOW AND TRANSPORT STUDIES

4.3.1 Introduction

As was discussed in previous sections, analyses were conducted to evaluate the effects of potash mining on WIPP repository parameters which might potentially affect the migration of radionuclides to the accessible environment. Of primary concern is the potential for an increase in hydraulic conductivity of the Culebra due to collapse of underground mines inside the WIPP Land Withdrawal Boundary. It is important to keep in mind that this work was performed following that presented in Section q of EPA's Background Information Document (Docket: a-93-02, II-G-1, Ref. #239), yet prior to DOE's submittal of the CCA. Therefore, the parameters that were selected for the modeling are consistent with those used by DOE in the 1992 PIA. In some instances, this report has been revised to link the approach taken here to that used in the CCA. A discussion of DOE's overall approach in the CCA is provided in Secion b.

Two types of calculations were performed in this analysis. As is presented in Section 4.2, the first involved the use of a rock mechanics model to estimate the amount of strain that could occur within the WIPP site due to a collapsed mine. The strain computed by the rock

mechanics model was in turn used to calculate the subsequent increase in hydraulic conductivity of the Culebra. A series of STAFF3D simulations were then performed to evaluate the effect of the increased hydraulic conductivity and fracture porosity on radionuclide transport within the Culebra. Both homogeneous and heterogeneous hydraulic conductivity distributions were simulated.

The objective of the STAFF3D modeling was to determine the impact of increased strain within the Culebra on radionuclide transport. A 0.005% strain (see section 4.2.3.2) was used to compute a new hydraulic conductivity and fracture porosity for the Culebra. A sensitivity analysis was performed to evaluate the effect of increased hydraulic conductivity over a wide range of conditions. The following model parameters were investigated: 1) number of fractures in the Culebra, 2) physical retardation (i.e., matrix diffusion), and 3) chemical retardation (i.e., K_d). Simulations were performed for both homogeneous and heterogeneous distributions of hydraulic conductivity.

A series of nine different transport scenarios were simulated for the current hydraulic conductivity of the Culebra. Nine identical simulations, with the exception of the incorporation of strain effects on hydraulic conductivity, were performed for the case where the hydraulic conductivity is impacted by mining. The first eighteen transport simulations assumed a homogeneous distribution of hydraulic conductivity. An additional eighteen simulations were performed for a heterogeneous distribution of hydraulic conductivity.

4.3.2 Problem Conceptualization

The conceptual model for the mining calculations consisted of horizontal two-dimensional steady-state flow within the Culebra as was the case for both the 1992 PA and the CCA. The repository has been decoupled from the Culebra; meaning that the repository is a source of contaminant mass in the Culebra but fluid flow from the repository is considered negligible. In this manner, the flow of water from the repository into the Culebra does not affect groundwater velocities in the Culebra. A constant concentration source term was used in the model to introduce radionuclides (plutonium) into the Culebra. Free-water diffusion and distribution coefficients were chosen to simulate the migration of plutonium because several plutonium isotopes have exceedingly long half-lives which essentially removes the complications that radioactive decay would introduce into the analysis. The model domain covers the WIPP land withdrawal area which is four miles on each side (i.e., 16 mi^2).

Both homogeneous and heterogeneous steady-state flow simulations were performed. In the

simulations where the hydraulic conductivities of the Culebra were assumed to be homogeneous, the flow system is uniform and is essentially one-dimensional. The uniform steady-state velocity is parallel to the X direction in the model. The X direction is oriented from north to south, which is the prevailing direction of groundwater flow within the Culebra.

In the simulations where heterogeneity was added to the hydraulic conductivity field, the flow becomes two dimensional in the X and Y directions. Even though a three-dimensional model is used in these analyses, there are no vertical hydraulic gradients in the system. These are the same assumptions that are used in the SECO modeling for the 1992 PA and CCA.

In the mining-altered rock property scenarios, a strain of 0.005% was assumed to cover the entire area within the WIPP land withdrawal boundary. Thus, the simulations of post-mining conditions assumed that the hydraulic conductivity and fracture porosity were modified throughout the entire model domain.

Physical Retardation

Diffusion in solutions is the process whereby ionic or molecular constituents move under the influence of their kinetic activity in the direction of decreasing concentration gradient. The diffusion of radionuclides from water moving within fractures into and out of the rock matrix can significantly retard the rate of transport of the dissolved radionuclides, particularly for non-sorbing or low-sorbing soluble species. The apparent diffusion coefficient for a given radionuclide depends on properties that are intrinsic to the chemical species (e.g., mobility) as well as rock or porous medium properties (such as porosity, tortuosity, and sorption ratios).

In fractured systems, the potential whereby matrix diffusion allows interaction between the fracture and the matrix is described by the ratio of the fracture surface area to the bulk volume of the matrix. For the STAFF3D and SECO modeling in both the 1992 PA and CCA, this ratio is based on horizontal fractures aligned as parallel plates. The Sensitivity of transport to physical retardation is discussed in Section 4.3.4.1.

Chemical Retardation

In addition to the physical processes, the transport of radionuclides is affected by chemical processes. The following is a brief summary of the geochemical processes that could potentially play a role in the transport of radionuclides and is provided to offer an appreciation of their wide variety and complexity:

- Sorption — the attachment of chemical species on mineral surfaces by such processes as ion exchange, chemisorption, van der Waals attraction, etc., or ion exchange within the crystal structure.

- Ion exchange phenomena — that type of sorption restricted to interactions between ionic contaminants and geologic materials with charged surfaces which can retard the migration of radionuclides.

- Speciation — the distribution of a given constituent among possible chemical forms of the radionuclide can influence its solubility and therefore its rate of transport by limiting the maximum concentration of the element dissolved in the aqueous phase.

- Precipitation — the process by which dissolved species exceed solubility limits, resulting in a portion precipitating out of solution.

- Natural colloidal formation — the attachment of radionuclides to colloids resulting in a mode of radionuclide transport or retardation which involves the movement or mechanical retardation of radionuclides attached to large colloidal particulate matter suspended in the groundwater or the formation of colloidal clusters of radionuclide molecules.

- Radiolysis — the change in speciation due to radiation or recoil during radioactive decay, which can affect the solubility of radionuclides.

- Biofixation — the binding of radionuclides to the soil/organic matrix due to the action of some types of microorganisms and plants, thus affecting mobility of the radionuclide.

- Natural organic matter interactions — soil organic matter can play a significant role in mobilizing, transporting, sorbing, and concentrating certain radionuclides.

- Anion exclusion — negatively charged rock surfaces can affect the movement of anions, by either retarding the movement of anions by not allowing negatively charged radionuclides to pass through the pore opening, or by enhancing the transport of ions by restricting the anion movement to the center of the pore channel where groundwater velocities are higher.

Obviously, a wide range of complex geochemical reactions can affect the transport of

radionuclides. Many of these reactions are poorly understood and are primarily research topics. From a practical view, the important aspect is the removal of solute from solution, irrespective of the process. For this reason, most computer codes simply lump all of the cumulative effects of the geochemical processes into a single term (i.e., distribution coefficient) which describes the degree to which the radionuclide is retarded relative to the groundwater. Thus, the distribution coefficient (K_d) relates the radionuclide concentration in solution to concentrations adsorbed to the rock. Use of K_d is the simplest mathematical approach to adsorption and values may be derived from the Freundlich isotherm equation

where *x/m* is the amount adsorbed (Ci chemical per gram of rock), and *C* is the concentration of chemical Ci/ml in the aqueous phase.

As mentioned previously in Section 4.1, Darcy's law relates the movement of water in a porous medium to the hydraulic gradient and the hydraulic conductivity. The hydraulic conductivity is a measure of the transmissive capacity of the medium coupled with the density and viscosity of the fluid (saline water in this case). The hydraulic gradient is simply the slope of the water table (unconfined aquifers) or the potentiometric surface for a confined system.

The advective flow rate for a conservative contaminant (i.e., non-sorbing and nonreactive) migrating through a porous medium is computed by dividing the Darcy velocity by the effective porosity.

Estimating radionuclide transport velocity is based on estimating the velocity of groundwater. For those radionuclides that flow with the water, contaminant velocity equals water velocity. For those that flow at rates that differ from water, the estimated water velocity must be divided by a retardation factor to approximate the contaminant velocity as described below.

The distribution coefficient is used to calculate a retardation factor (R_F) as determined from the following equation:

where K_d is the distribution coefficient; P_b is the bulk density of the aquifer material; and n_e is the aquifer effective porosity. The retardation factor is the ratio between the groundwater and radionuclide velocities. For instance, a retardation factor of 2, indicates that the groundwater moves at twice the rate of the radionuclide. The sensitivity of radionuclide transport to chemical retardation is discussed in Section 4.3.4.1.

4.3.3 Model Formulation

The STAFF3D grid used for these calculations consisted of 30,000 nodes and 19,602 elements in 3 planes. The grid spacing was a constant 63 meters in both the X and Y directions. The vertical dimension was a constant 7.7 m (i.e., the average thickness of the Culebra dolomite).

Boundary conditions for the grid consisted of fixed head boundaries at the upgradient and downgradient ends of the model. The heads were chosen to provide a gradient across the model of 0.0032 m/m. This value was computed from available water-level data measured in the Culebra in the vicinity of WIPP. The lateral edges and the bottom of the model were assumed to be no-flow boundaries. As in the 1992 PA, areal recharge to the Culebra was assumed to be zero.

4.3.3.1 Homogeneous Hydraulic Conductivity Simulations

In the 1992 PA it was assumed that the median hydraulic conductivity of the Culebra is 7 m/y (Docket: A-93-02, Ref. #563, Vol. 4, p 5-7). As voted previously this value was reduced to 4.0m for the CCA. Therefore, all homogeneous simulations in this analysis also assumed an equivalent hydraulic conductivity of 7 m/y within a dual-porosity medium. The methods outlined in Section 4.1 were used to determine values of fracture hydraulic conductivity and fracture porosity at fracture spacings which represent 1, 10, and 100 fractures in the Culebra. These values are shown in Table 4-3 for both the undisturbed and post-mining scenarios. The number of fractures is used in the simulation nomenclature to distinguish individual simulations from one another (i.e, 1, 10, or 100).

Table 4-3. Hydraulic Conductivities and Fracture Porosity for Homogeneous Simulations.

Number of Fractures	Strain (%)	Fracture K (m/y)	Fracture Porosity	Equivalent Hydraulic Conductivity (m/y)
1	NA	421,240	1.66E-05	7.0
10	NA	90,750	7.71E-05	7.0
100	NA	19,550	3.58E-04	7.0
1	.005	6,770,800	6.66E-05	451.0
10	.005	246,600	1.27E-04	31.4
100	.005	25,400	4.08E-04	10.4

Transport parameters were also assumed to be homogeneous (H) and are summarized in Table 4-4. Three different transport scenarios were performed. In the first type, the contaminant was assumed to be a conservative tracer with no matrix diffusion, no retardation, and no radioactive decay. Note that this first set consists of six transport simulations, those that were performed without an induced strain (1H, 10H, and 100H) and those in which a strain (S) of 0.005% has been applied (1HS, 10HS and 100HS). In the second type of simulations, the lowest value of matrix diffusion (D) reported for plutonium in the 1992 PA (1.514×10^{-3} m^2/y) was assumed in both the unstrained case (i.e., 1HD, 10HD and 100HD) and the scenarios in which 0.005% strain was applied (i.e., 1HDS, 10HDS and 100HDS). In the final set of simulations, the lowest value of K_d (10^{-4} m^3/kg) for plutonium reported in the 1992 PA was used to compute a retardation factor (R_F) which was applied to both the unstrained (1HDR, 10HDR and 100HDR) and strained cases (1HDRS, 10HDRS, 100HDRS).

It is important to realize that regardless of whether the unstrained system was assumed to have 1, 10, or 100 fractures the equivalent porous media hydraulic conductivity value will always equal 7 m/y (Table 4-3). This makes sense from a perspective that this equivalent porous media hydraulic conductivity is an average value obtained from field aquifer tests. The field test results are transparent to the actual number of fractures, and therefore all that is known is that their sum total effect, results in an equivalent hydraulic conductivity of 7 m/y. An extension of the parallel plate theory explained in Section 4.1 is that the fracture hydraulic conductivity multiplied by the fracture porosity is always equal to the equivalent hydraulic conductivity (Table 4-3).

Table 4-4. Input Parameters for Homogeneous Hydraulic Conductivity Simulations.

	1H, 10H, 100H 1HS, 10HS, 100HS	1HD, 10HD, 100HD 1HDS, 10HDS, 100HDS	1HDR, 10HDR, 100HDR 1HDRS, 10HDRS, 100HDRS
RADIONUCLIDE — Pu-239			
K_d (m^3/kg)	0.0	0.0	0.0001
Diff. Coeff. (m^2/y)	0.0	1.54E-03	1.54E-03
Half life (y)	no decay	no decay	no decay
CULEBRA Matrix Properties			
Retardation Factor	1	1	2.75
Effective Porosity	0.139	0.139	0.139
Specific Storage (m^{-1})	*NA	NA	NA
Hyd. conductivity (m/y)	7.0	7.0	7.0
Tortuosity	0.0	0.0	0.0
Fluid Density (kg/m^3)	1020	1020	1020
CULEBRA Fracture Properties			
Retardation Factor	1	1	1
Fluid Density (kg/m^3)	1020	1020	1020
Hyd. Conductivity (m/y)	See Table 4-3	See Table 4-3	See Table 4-3
Tortuosity	0.0	0.0	0.0
Fracture spacing (m) (single)	See Table 4-3	See Table 4-3	See Table 4-3
Fracture Porosity	See Table 4-3	See Table 4-3	See Table 4-3
Porosity within Fractures	1	1	1
Specific Storage (m^{-1})	NA	NA	NA
Long. Dispersivity (m)	25.0	25.0	25.0
Ratio of (long/transv.) Disp.	10:1	10:1	10:1

* Not Applicable

It is also shown in Table 4-3 that once strain is assumed to have altered the hydraulic conductivities, the equivalent hydraulic conductivity varies with the number of fractures. This is because the strain is assumed to increase the fracture(s) aperture, and since one does not know how many fractures are actually in the Culebra, the approach taken here is to present several possible fracture spacings over which the strain is dissipated (i.e., 1, 10, 100). If only one fracture is assumed, all of the strain is exerted on that single fracture. Since the hydraulic conductivity is a function of the cube of the fracture aperture, a large change in a single fracture aperture will affect the equivalent hydraulic conductivity to a greater extent than a small change in many fracture apertures.

The 0.005% strain that was imposed on the transmissivity field resulted in a homogeneous field with an equivalent hydraulic conductivity of either 451, 31.4 or 10.4 m/y for 1, 10, or 100 fractures, respectively. Of particular interest is that as the number of fractures increases, the equivalent conductivity of the strained medium approaches the porous media or

equivalent hydraulic conductivity value of 7 m/y. This concept is further illustrated by Figure 4-14 which shows how the equivalent hydraulic conductivity approaches 7 m/y as the fracture frequency increases.

4.3.3.2 Heterogeneous Hydraulic Conductivity Simulations

A second set of 18 dual-porosity transport simulations were performed using a heterogeneous distribution of transmissivities based on a composite of the 70 transmissivity fields used in the 1992 PA (Docket: A-93-02, Ref. #563). As was the case in the homogeneous simulations, three different values of fractures in the Culebra were used (i.e., 1, 10, and 100).

Heterogeneous Hydraulic Conductivity at Ambient Strain

Implementing the heterogeneous distribution for hydraulic conductivity involved a series of transformations from the 1992 PA data to the STAFF3D input files. The first step was to transform the transmissivity data from a regional model grid used in the 1992 PA to the local grid used for the STAFF3D modeling. The regional distribution of transmissivity in the Culebra is shown in Figure 4-15. Note that the transmissivity data includes areas outside the WIPP land withdrawal boundary and that the model grid has been rotated by 38 degrees west of north.

A simple coordinate transformation was used to map the regional transmissivity data on the local grid used by STAFF3D. The resulting transmissivity distribution for the STAFF3D model domain is shown in Figure 4-16. Visual inspection of the contoured transmissivity field can verify that the data have been mapped correctly.

Figure 4-14. Equivalent Porous Matrix Hydraulic Conductivity Computed for a Strain of 0.005%

The transmissivity data were transformed from Log_{10} T in units of m^2/s to hydraulic conductivity in units of m/y by dividing the transmissivity data by the thickness of the Culebra (7.7 m) and by multiplying by a constant for the unit conversion. The computed hydraulic conductivity data are contoured for the STAFF3D model domain in Figure 4-17. The hydraulic conductivity data range from a low of about 2 m/y to a high of approximately 500 m/y over the model domain. This may be compared to the 7 m/y value used for the homogeneous case (Section 4.3.3.1).

Figure 4-15. Composite Transmissivity Field from Intera (Log_{10} T m^2/s).

STAFF3D implements heterogeneous hydraulic conductivity distributions by assigning a material type to each element in the model. A material type is an integer number that denotes a particular value of hydraulic conductivity. Due to the large number of elements in the STAFF3D model, it was not practical to assign a unique hydraulic conductivity value to each element. Therefore, a set of 8 material types were defined having equivalent porous hydraulic conductivity values of 2, 5, 10, 20, 50, 100, 200, and 500 m/y.

Figure 4-16. Interpolated Transmissivity Distribution (Log_{10} T m^2/s).

These values were chosen to be approximately evenly spaced on a logarithmic scale. For example, if an equivalent porous media hydraulic conductivity obtained from the composite hydraulic conductivity field indicated that a particular block within the model domain should be assigned a hydraulic conductivity of 18 m/y, this value would subsequently be rounded to an equivalent hydraulic conductivity of 20 m/y.

Figure 4-17. Unstrained Hydraulic Conductivity Distribution (m/y) over WIPP Site.

The final step was to compute the fracture hydraulic conductivity and fracture porosity for the porous media hydraulic conductivity values described above. This calculation was performed assuming 1, 10, and 100 fractures. Values are shown in Table 4-5 for both the undisturbed and strain-altered scenarios. It is important to recognize that, as was seen earlier with the homogeneous case, regardless of whether the system is assumed to have 1, 10 or 100 fractures, the equivalent porous media conductivity value associated with that region of the model (i.e., 2, 5, 10, 20, 50, 100, 200, or 500 m/y) will always be the same. Therefore, only one hydraulic conductivity field is required to show the equivalent porous media hydraulic conductivities for the unstrained heterogeneous simulations (Figure 4-17).

Transport parameters for the heterogeneous simulations are summarized in Tables 4-5 and 4-6. The three types of transport scenarios performed for the heterogeneous (T) simulations

were identical to those performed for the homogenous simulations. Namely, the case where there is no matrix diffusion, no retardation, and no radioactive decay (1T, 10T, and 100T); the second type where the lowest value of matrix diffusion (D) reported for plutonium in the 1992 PA is assumed (i.e., 1TD, 10TD and 100TD); and the final case, where the lowest value of K_d reported in the 1992 PA for plutonium was used to compute a retardation factor (R) which is applied in simulations 1TDR, 10TDR and 100TDR. For additional information pertaining to distribution coefficients see A-93-02, V-B-4 and V-B-7.

Heterogeneous Transmissivities Influenced by Strain

The transmissivities that are affected by a 0.005% strain were processed in a similar manner to those for the heterogeneous unstrained scenario, in that the transmissivity data were transformed from the regional model grid to the local grid and then converted to hydraulic conductivities by dividing by the Culebra thickness of 7.7 m.

As mentioned previously, in the case of the transmissivities at ambient strain, the equivalent hydraulic conductivities will be the same for each of the respective model elements (i.e., 2, 5, 10, or 500 m/y) regardless of the number of fractures. However, this is not the case when the 0.005 % strain is assumed to open either 1, 10 or 100 fractures. This is because the relationship of the fracture aperture to the hydraulic conductivity is nonlinear, therefore the effect on hydraulic conductivity of increasing the aperture of a single fracture is significantly different than from distributing the same amount of strain to numerous fractures.

It was assumed that the number of fractures in the Culebra are somewhere between 1 and 100. Furthermore, it was also assumed that the strain applied to the system, would not create more fractures but only to open up existing fractures. This assumption, and the nonlinear relationship of the hydraulic conductivity to the number of fractures leads to equivalent hydraulic conductivities that are dependent on the number of fractures. The computed values of hydraulic conductivity calculated at a strain of 0.005% are summarized in Table 4-5.

Table 4-5. Hydraulic Conductivities and Porosity Values Used in Heterogeneous Simulations.

Equivalent K (m/y)	Unaltered Parameters			Strain Altered Parameters			Equivalent K (m/y)
	Number of Fractures	Fracture K (m/y)	Fracture Porosity	Number of Fractures	Fracture K (m/y)	Fracture Porosity	
2	1	182,700	1.09E-05	1	5,666,400	6.09E-05	345
	10	39,400	5.08E-05	10	155,000	1.01E-04	15.6
	100	8,480	2.36E-04	100	12,400	2.86E-04	3.56
5	1	336,600	1.49E-05	1	6,416,000	6.49E-05	416
	10	72,500	6.89E-05	10	215,900	1.19E-04	25.7
	100	15,600	3.20E-04	100	20,900	3.70E-04	7.73
10	1	534,300	1.87E-05	1	7,203,000	6.87E-05	495
	10	115,100	8.69E-05	10	285,800	1.37E-04	39.1
	100	24,800	4.03E-04	100	31,300	4.53E-04	14.2
20	1	848,200	2.36E-05	1	8,258,500	7.36E-05	608
	10	182,700	1.09E-04	10	387,800	1.59E-04	61.8
	100	39,400	5.08E-04	100	47,500	5.58E-04	26.5
50	1	1,562,300	3.20E-05	1	10,256,900	8.20E-05	841
	10	336,600	1.48E-04	10	601,300	1.99E-04	119
	100	72,500	6.90E-04	100	83,400	7.40E-04	61.7
100	1	2,480,000	4.03E-05	1	12,441,600	9.03E-05	1120
	10	534,300	1.87E-04	10	858,000	2.37E-04	203
	100	115,100	6.90E-04	100	128,800	9.19E-04	118
200	1	3,936,900	5.08E-05	1	15,500,800	1.01E-04	1560
	10	848,200	2.36E-04	10	1,245,900	2.86E-04	356
	100	182,700	1.09E-03	100	199,900	1.14E-03	229
500	1	7,251,800	6.90E-05	1	21,587,300	1.19E-04	2570
	10	1,562,300	3.20E-04	10	2,088,300	3.70E-04	773
	100	336,600	1.48E-03	100	359,600	1.54E-03	552

STAFF3D simulations for the heterogeneous strained case are analogous to the unstrained simulations, except that the simulations incorporate the heterogeneous distribution of hydraulic conductivity that has been modified using a strain of 0.005%. As shown in Table 4-6, an "S" is used in the nomenclature to indicate that a strain has been applied.

Unlike the unstrained case where one hydraulic conductivity field describes the hydraulic conductivity for all three fracture sets, three separate fields are required to illustrate the hydraulic conductivities. Hydraulic conductivity fields assuming 1, 10, and 100 fractures are shown in Figures 4-18, 4-19 and 4-20, respectively.

Table 4-6. Input Parameters for Heterogeneous Hydraulic Conductivity Simulations.

	Simulations		
	1T, 10T, 100T 1TS, 10TS, 100TS	1TD, 10TD, 100TD 1TDS, 10TDS, 100TDS	1TDR, 10TDR, 100TDR 1TDRS, 10TDRS, 100TDRS
RADIONUCLIDE — Pu-239			
K_d (m^3/kg)	0.0	0.0	0.0001
Diff. Coeff. (m^2/y)	0.0	1.54E-03	1.54E-03
Half life (y)	no decay	no decay	no decay
CULEBRA Matrix Properties			
Retardation Factor	1	1	2.75
Effective Porosity	0.139	0.139	0.139
Specific Storage (m^{-1})	NA	NA	NA
Hyd. conductivity (m/y)	7.0	7.0	7.0
Tortuosity	0.0	0.00	0.0
Fluid Density (kg/m^3)	1020	1020	1020
CULEBRA Fracture Properties			
Retardation Factor	1	1	1
Fluid Density (kg/m^3)	1020	1020	1020
Hyd. Conductivity (m/y)	See Table 4-5	See Table 4-5	See Table 4-5
Tortuosity	0.0	0.0	0.0
Fracture Frequency (m) (single)	See Table 4-5	See Table 4-5	See Table 4-5
Fracture Porosity			
Porosity within Fractures	See Table 4-5	See Table 4-5	See Table 4-5
Specific Storage (m^{-1})	1	1	1
Long. Dispersivity (m)	NA	NA	NA
Ratio of (long/transv.) Disp.	25 1:10	25 1:10	25 1:10

[1] Not Applicable

4.3.4 Description of Simulations

The simulations were evaluated in two ways. First, breakthrough curves were created for each transport simulation. Relative concentrations were plotted versus time at four locations downgradient from the source area. These locations are 0.2, 1.0, 1.6, and 2.4 km downgradient and in the center of the plume. The maximum relative concentration would be 1.0, which is the value specified at the source node. All of these breakthrough curves are provided in Appendix A.

The second evaluation method was chosen to simplify the comparison between the various runs. The contaminant breakthrough data were summarized (Table 4-7) at a distance of 2.4 km downgradient from the source (i.e., at the WIPP land withdrawal boundary). For each simulation, the following information is reported: 1) the time to reach a relative concentration of 1 x 10^{-5}, 2) the maximum relative concentration attained after 10,000 years,

and 3) the time to reach a relative concentration that is ninety percent of the maximum concentration (called the breakthrough time). To facilitate the intercomparison between various scenarios, the following discussion presents selected results from the most relevant simulations in order to illustrate the effect that strain may have on the groundwater flow and radionuclide transport.

4.3.4.1 Comparison of Homogeneous Simulations

Homogeneous simulations under ambient strain and subsidence-altered strain conditions were performed for three cases, each with 1, 10 and 100 fractures. The three cases are: 1) radionuclides are not physically or chemically retarded; 2) radionuclides are only retarded by physical means (i.e., matrix diffusion) and; 3) radionuclides are both physically and chemically retarded. The results from these simulations provide insight not only into the overall effects that strain may have on the radionuclide transport but also into the relative importance of physical and chemical retardation relative to potential strain effects.

Although all of the simulations were performed with 1, 10 and 100 fractures, as noted earlier it is considered so improbable that a single fracture stretches the 2.4 miles from the proposed repository to the WIPP land withdrawal boundary that the primary focus of the following discussion is placed on the 10 and 100 fracture scenarios. However, the results from the single fracture scenarios assuming homogeneous hydraulic conductivity are presented in Table 4-8 and in the appendices.

Sensitivity to Number of Fractures

In Figure 4-21 and Table 4-8, the modeling results indicate that in the *un*strained case where there is no matrix diffusion, radioactive decay or chemical retardation, the contaminants reach the WIPP land withdrawal boundary at approximately the same time independent from the number of fractures. This observation ties back to the discussion in Section 4.3.3.1 which indicates that regardless of whether the *un*strained system is assumed to have 1, 10 or 100 fractures the equivalent hydraulic conductivity will always be equal to the assigned porous media hydraulic conductivity of 7 m/y. Therefore, the groundwater velocity will be the same in all three scenarios since all of the input parameters, including the hydraulic conductivity, are essentially the same.

Figure 4-18. Strain Altered Hydraulic Conductivity Values Over WIPP Site for 1 Fracture.

Figure 4-19. Strain Altered Hydraulic Conductivity Values Over WIPP Site for 10 Fractures.

Figure 4-20. Strain Altered Hydraulic Conductivity Values Over WIPP Site for 100 Fractures.

Table 4-7. Summary of Relative Concentration Breakthrough at a Distance of 2.4 km Downgradient of the Source (WIPP Land Withdrawal Boundary).

Simulation	Fractures	Diffusion Coeff.(m2/y)	K_d	Strain (%)	K	Time (yr) to Reach 1.00E-05	Time (yr) to Reach Breakthrough	Max Conc.
1H[1]	1	0.0	0.0	0.000	Homogeneous	160	600	0.251
1HS[2]	1	0.0	0.0	0.005	Homogeneous	2.9	8.8	0.183
1T[3]	1	0.0	0.0	0.000	Heterogeneous	30	90	0.05
1TS	1	0.0	0.0	0.005	Heterogeneous	1.5	4.2	0.044
10H	10	0.0	0.0	0.000	Homogeneous	160	600	0.183
10HS	10	0.0	0.0	0.005	Homogeneous	38	130	0.183
10T	10	0.0	0.0	0.000	Heterogeneous	30	85	0.07
10TS	10	0.0	0.0	0.005	Heterogeneous	10	29	0.056
100H	100	0.0	0.0	0.000	Homogeneous	200	600	0.183
100HS	100	0.0	0.0	0.005	Homogeneous	120	420	0.183
100T	100	0.0	0.0	0.000	Heterogeneous	35	100	0.07
100TS	100	0.0	0.0	0.005	Heterogeneous	25	75	0.051
1HD[4]	1	1.54E-03	0.0	0.000	Homogeneous	2550	24,000	0.183
1HDS	1	1.54E-03	0.0	0.005	Homogeneous	2.9	750	0.183
1TD	1	1.54E-03	0.0	0.000	Heterogeneous	110	4500	0.05
1TDS	1	1.54E-03	0.0	0.005	Heterogeneous	1.7	270	0.044
10HD	10	1.54E-03	0.0	0.000	Homogeneous	6100	21,300	0.183
10HDS	10	1.54E-03	0.0	0.005	Homogeneous	1300	4450	0.183
10TD	10	1.54E-03	0.0	0.000	Heterogeneous	1000	3100	0.07
10TDS	10	1.54E-03	0.0	0.005	Heterogeneous	300	1000	0.056
100HD	100	1.54E-03	0.0	0.000	Homogeneous	6150	21,300	0.183
100HDS	100	1.54E-03	0.0	0.005	Homogeneous	4150	14,300	0.183
100TD	100	1.54E-03	0.0	0.000	Heterogeneous	1100	3100	0.07
100TDS	100	1.54E-03	0.0	0.005	Heterogeneous	830	2200	0.051
1HDR[5]	1	1.54E-03	1.00E-04	0.000	Homogeneous	7000	NA	0.109
1HDRS	1	1.54E-03	1.00E-04	0.005	Homogeneous	8	2030	0.183
1TDR	1	1.54E-03	1.00E-04	0.000	Heterogeneous	270	8400	0.04
1TDRS	1	1.54E-03	1.00E-04	0.005	Heterogeneous	4.5	700	0.044

Table 4-7 (Continued)

Simulation	Fractures	Diffusion Coeff.(m2/y)	K_d	Strain (%)	K	Time (yr) to Reach 1.00E-05	Time (yr) to Reach Breakthrough	Max Conc.
10HDR	10	1.54E-03	1.00E-04	0.000	Homogeneous	16,700	NA	0.114
10HDRS	10	1.54E-03	1.00E-04	0.005	Homogeneous	3600	13,000	0.183
10TDR	10	1.54E-03	1.00E-04	0.000	Heterogeneous	2900	8600	0.07
10TDRS	10	1.54E-03	1.00E-04	0.005	Heterogeneous	830	2750	0.056
100HDR	100	1.54E-03	1.00E-04	0.000	Homogeneous	16,800	NA	0.113
100HDRS	100	1.54E-03	1.00E-04	0.005	Homogeneous	11,300	39,000	0.18
100TDR	100	1.54E-03	1.00E-04	0.000	Heterogeneous	3100	8500	0.07
100TDRS	100	1.54E-03	1.00E-04	0.005	Heterogeneous	2200	6000	0.051

[1] Homogeneous hydraulic conductivities
[2] Strain applied (.005%)
[3] Heterogeneous hydraulic conductivities
[4] Matrix diffusion is simulated
[5] Chemical retardation is simulated

Table 4-8. Selected Results from Homogeneous Hydraulic Conductivity Simulations Without Physical or Chemical Retardation

1 Fracture		
Simulation	Strain	Time (Yr) to Reach 1.00E-05
1H	No	160
1HS	Yes	2.9

10 Fractures		
Simulation	Strain	Time (Yr) to Reach 1.00E-05
10H	No	160
10HS	Yes	38

100 Fractures		
Simulation	Strain	Time (Yr) to Reach 1.00E-05
100H	No	200
100HS	Yes	120

In the strained system, however, the number of fractures over which the 0.005% strain is distributed makes a significant difference in the arrival times of the radionuclides, as shown in Figure 4-22 and Table 4-8. As was also previously discussed, this effect occurs because of the nonlinear relationship between increases in fracture aperture and equivalent hydraulic conductivity. In the case where all of the strain displacement (i.e., aperture opening) was placed on one fracture, the equivalent hydraulic conductivity is about 450 m/y; whereas if this strain is distributed over 100 fractures the resulting equivalent hydraulic conductivity is 10.4 m/y (Table 4-3 and Figure 4-14). Therefore, radionuclide arrival at the land withdrawal boundary for the single fracture scenario occurs at a much earlier time than for the 100 fracture case (2.9 *vs* 120 years). Also of interest is that as the number of fractures increases, the difference between the unstrained and strained results becomes less significant (Figure 4-22). For example, the difference between the arrival times for the single fracture *un*strained versus strained scenario is 160 and 2.9 years, or a factor of about 55 (Table 4-8). Whereas a similar comparison made on the 10 and 100 fracture scenario indicates that the difference is a factor of about 4.2 (160 divided by 38) and about 1.7 (200 divided by 120), respectively.

Figure 4-21. Unstrained Homogenous Hydraulic Conductivity Simulations Without Physical or Chemical Retardation.

Again, this phenomenon is due to the relationship illustrated in Figure 4-14, where it is shown that, as the number of fractures increases, the effect of strain eventually diminishes to a situation where the equivalent hydraulic conductivity approaches that of the porous media or, in the case of the homogeneous simulations, 7 m/y.

Keeping in mind that the following conservative assumptions have been used in the modeling, it appears reasonable to conclude that for the homogeneous case, without physical or chemical retardation, it is unlikely that the strain imposed by mining would increase the radionuclide velocities by more than a factor of 5 for the given boundary conditions.

- The hydraulic gradient is generally inversely related to the hydraulic conductivity. Therefore, since the hydraulic conductivity that is used in both the *un*strained and stained scenarios is calculated from *un*strained rock properties it is probably overestimated for the strained scenarios. This overestimation would lead to greater differences between the strained and unstrained values than would actually be present.

- The assumption that all of the imposed strain is effective at enlarging existing fractures rather than either opening new fractures or being dissipated by the matrix, is also conservative in that it will tend to maximize the fracture apertures and accentuate the difference between *un*strained and strained velocities.

- A factor of 5 assumes that a fracture frequency of 10 describes the entire domain, however, if any portion of the domain along the flow path is either unfractured or fractured at a density greater than 10, the results between the *un*strained and the strained scenarios would be closer than a factor of 5.

The following simulations involving physical and chemical retardation were performed to determine whether a factor of 5 difference between the *un*strained and strained scenarios is maintained when physical and chemical retardation are active.

Sensitivity to Physical Retardation

To evaluate the effect that matrix diffusion would have on radionuclide transport, a series of simulations were performed in which all of the model inputs are identical to the previous homogeneous simulations, only now either a high or low diffusion rate is assigned to match those used to bound plutonium in the 1992 PA (1.514×10^{-3} - 9.4×10^{-3} m^2/y).

Figure 4-22. Strained and Unstrained Homogenous Hydraulic Conductivity Simulations Without Physical or Chemical Retardation.

Figure 4-23 shows a comparison of a 10 and 100 fracture system under strained and unstrained conditions when a low diffusion rate (1.514×10^{-3} m^2/y) is considered. As would be expected, radionuclides are first to reach the land withdrawal boundary in the simulation involving 10 fractures under strained conditions (1300 yrs). The simulation with the next fastest arrival time is the 100 fracture strained case (4150 yrs).

Of particular interest are the similar radionuclide breakthrough times for the 10 and 100 fracture simulations in which matrix diffusion is simulated, 6100 versus 6150, respectively. One would expect that a greater number of fractures would enhance the physical retardation because of an increase in the fracture surface area over which diffusion into the rock matrix may take place. In fact, this relationship is evident from a comparison of the radionuclide arrival times from a single *un*strained fracture with diffusion versus the arrival times based on 10 *un*strained fractures in which diffusion is also considered (Table 4-7). As shown previously in Figure 4-21, without diffusion the radionuclide breakthrough curves for 1, 10 and 100 fractures are very similar and fall between 160 and 200 years. Now with the addition of matrix diffusion, radionuclide breakthrough does not occur in the single fracture scenario until 2550 years, 6100 years for the 10 fracture scenario, and 6150 years for 100 fractures.

To determine the sensitivity of the results to matrix diffusion, an additional simulation was performed in which the highest value for diffusion assigned in the 1992 PA was used (i.e., 9.4 x 10-3 m^2/y). As shown in Figure 4-24, the results are insensitive to the value of matrix diffusion once the number of fractures exceeds 10.

This insensitivity of contaminant breakthrough times to diffusion for 10 or more fractures was investigated by comparing the radionuclide concentrations within the matrix block to concentrations in the fracture at early simulation times. These analyses revealed that the radionuclide concentrations within the matrix block reach equilibrium with the fracture in less than 1,800 years. Once equilibrium is established, no further diffusion takes place because the source is constant and the plume reaches and maintains a steady-state concentration. Thus as the matrix blocks become smaller for a greater number of fractures, the value of the diffusion coefficient loses sensitivity in a constant-source problem.

Figure 4-23. Homogenous Hydraulic Conductivity Simulations with Physical Retardation.

To facilitate an evaluation of the effects of matrix diffusion on radionuclide transport the results from selected simulations are presented in Table 4-9. From these data it is apparent that the inclusion of matrix diffusion results in a 30 to 38 fold increase in the travel time. A comparison of strained versus unstrained values for 10 fractures indicates that, as in the case for which matrix diffusion is not considered, a factor of 5 decrease in travel time still holds when matrix diffusion is included (6100 divided by 1300). In the 100 fracture scenario, contaminant breakthrough times are only about 50 percent faster for the strain altered simulations (6150 divided by 4150).

Sensitivity to Chemical Retardation

To illustrate the sensitivity of radionuclide transport to chemical (i.e., K_d) retardation, the results from three simulations are presented in Figure 4-25. These results are from 10 fracture simulations in which: 1) physical and chemical retardation are inactive, 2) physical retardation is active but chemical retardation is not, and 3) both physical and chemical retardation are active. The modeling results indicate that it would take approximately 160 years for radionuclide breakthrough to occur at the land withdrawal boundary if physical and chemical retardation are not considered (Table 4-9). This arrival time increases to about 6100 years (Table 4-9), once matrix diffusion is included. As was noted earlier in Section 4.3.2, the amount of chemical retardation is dependent upon the distribution coefficient (K_d), bulk density and effective porosity of the matrix.

To obtain an estimate for chemical retardation, median parameter values for bulk density and effective porosity were selected from the 1992 PA, in conjunction with the lowest plutonium distribution coefficient. This combination of parameters resulted in a retardation factor (R_F) of 2.75. It is important to keep in mind that based on the parameter ranges presented in the 1992 PA the R_F could vary over a very wide range (i.e, 1.8 to 2,715,790). (Note: At the time of this analysis, insufficient evidence has been presented to EPA to support the use of chemical retardation in DOE's Performance Assessment).

To facilitate an evaluation of the effects of chemical retardation on radionuclide transport the results from selected simulations are presented in Figure 4-26 and Table 4-10. From these data it is apparent that the inclusion of chemical retardation results in approximately a 2.7 decrease in the travel time. Since the R_F is linearly related to the radionuclide velocity it is not

Figure 4-24. Homogeneous Hydraulic Conductivity Simulations with High and Low Values of Diffusion.

Table 4-9. Selected Results from Homogeneous Hydraulic Conductivity Simulations with Physical Retardation.

10 Fractures			
Simulation	Strain	Diffusion	Time (Yr) to Reach 1.00E-05
10H	No	No	160
10HD	No	Yes	6100
10HS	Yes	No	38
10HDS	Yes	Yes	1300

100 Fractures			
Simulation	Strain	Diffusion	Time (Yr) to Reach 1.00E-05
100H	No	No	200
100HD	No	Yes	6150
100HS	Yes	No	120
100HDS	Yes	Yes	4150

surprising that an R_F of 2.7 leads to travel times that are approximately 2.7 times longer than for a comparable simulation in which only matrix diffusion is considered.

A comparison of strained versus unstrained values for the 10 fracture scenario indicates that, as in the other cases that have been considered, a factor of 5 decrease in travel time still holds when chemical retardation is included (16700 divided by 3600). In the 100 fracture scenario, contaminant breakthrough times are about 50 percent faster for the strain altered simulations.

4.3.4.2 Comparison of Heterogeneous Hydraulic Conductivity Simulations

Heterogeneous simulations were evaluated in the same manner as the homogeneous simulations with the exception that the location of observation nodes was altered so that they remained in the center of the contaminant plume. In the homogeneous case, the observation points (those plotted on the breakthrough curves in Appendix A) were chosen to lie on the center-line of the plume. These observation points followed a straight line downgradient from the source node and parallel to the X-axis, because a uniform gradient was applied to the model in the homogeneous case. In the heterogeneous model, on the other hand, the distribution of hydraulic conductivity caused the plume to shift to the east, as shown in Figure 4-27. Thus, the observation nodes were chosen to be approximately the same distance

downgradient from

Figure 4-25. Homogeneous Hydraulic Conductivity Simulations Comparing the Effects of Physical and Chemical Retardation on Radionuclide Transport Times.

Figure 4-26. Homogeneous Hydraulic Conductivity Simulations that Include Physical and Chemical Retardation.

Table 4-10. Selected Results from Homogeneous Hydraulic Conductivity Simulations with Physical and Chemical Retardation.

10 Fractures				
Simulation	Strain	Diffusion	Sorption (K_d)	Time (Yr) to Reach 1.00E-05
10HD	No	Yes	No	6100
10HDR	No	Yes	Yes	16700
10HDS	Yes	Yes	No	1300
10HDRS	Yes	Yes	Yes	3600

100 Fractures				
Simulation	Strain	Diffusion	Sorption (K_d)	Time (Yr) to Reach 1.00E-05
100HD	No	Yes	No	6150
100HDR	No	Yes	Yes	16800
100HDS	Yes	Yes	No	4150
100HDRS	Yes	Yes	Yes	11300

the source but still within the center of the plume. The distance between the source and the land withdrawal boundary observation point, as summarized in Table 4-7, is actually about 2.6 km rather than 2.4 km for the homogeneous case.

Conclusions drawn from the heterogeneous simulations are similar to those of the homogeneous case. The greatest impact from mining is seen in the simulations of a single fracture. The differences in travel times, however, are not as great as in the homogeneous case as is shown in the following discussion.

Sensitivity to Number of Fractures

In Figure 4-28 and Table 4-11, the modeling results indicate that in the *un*strained case where there is no diffusion, radioactive decay or chemical retardation, the contaminants reach the WIPP land withdrawal boundary at approximately the same time (i.e., 35 years) independent of the number of fractures. This observation was also made for the homogeneous case and relates to the fact that, in the unstrained scenarios, regardless of the number of fractures the equivalent hydraulic conductivity is the same (Table 4-5).

Figure 4-27. Contaminant Plume for the Heterogeneous Simulation after 10,000 Years.

Figure 4-28. Heterogeneous Hydraulic Conductivity Simulations without Physical or Chemical Retardation.

Table 4-11. Selected Results from Heterogeneous Hydraulic Conductivity Simulations without Physical or Chemical Retardation.

1 Fracture		
Simulation	Strain	Time (Yr) to Reach 1.00E-05
1T 1TS	No Yes	30 1.5

10 Fractures		
Simulation	Strain	Time (Yr) to Reach 1.00E-05
10T 10TS	No Yes	30 10

100 Fractures		
Simulation	Strain	Time (Yr) to Reach 1.00E-05
100T 100TS	No Yes	35 25

As was true for the homogeneous case, the effects of strain in the heterogeneous simulations are dependent on the number of fractures (Table 4-11). As was also previously discussed, this effect occurs because of the nonlinear relationship between increases in fracture aperture and equivalent hydraulic conductivity.

Table 4-11 indicates that when matrix diffusion and chemical retardation are not considered, the difference between the strained and *un*strained arrival times are; a factor of 20 for a single fracture; a factor of 3, for 10 fractures and a factor of 1.4, for 100 fractures. These results are considered to represent maximum strain effects on radionuclide velocities for the same reasons as those provided for the homogeneous simulations (Section 4.3.4.1).

Sensitivity to Physical Retardation

In an identical fashion to the homogeneous simulations the effects of matrix diffusion on the heterogeneous transmissivity fields were evaluated. Complete results for all of the simulations are shown in Table 4-8 and in Appendix A.

Figure 4-29 shows a comparison of a 10 and 100 fracture system under strained and *un*strained conditions when a low diffusion rate ($1.514x10^{-3}$ m^2/y) is considered. As would be expected, radionuclides first reach the land withdrawal boundary in the simulation involving 10 fractures under strained conditions (300 yrs). The results for 100 fracture strained case indicate an arrival time of 830 years.

As was observed for the homogeneous case, the radionuclide breakthrough times for the 10 and 100 fracture simulations in which matrix diffusion is simulated, are very similar, 1000 versus 1100 years, respectively. As was previously explained, this insensitivity is due to the matrix block becoming sufficiently small that the value of diffusion is no longer a sensitive factor.

To facilitate an evaluation of the effects of matrix diffusion on radionuclide transport, the results from selected simulations are presented in Table 4-12. From these data it is apparent that the inclusion of matrix diffusion results in a 30 to 33 fold increase in the travel time. A comparison of strained versus *un*strained values for the 10 fracture scenario indicates that, as in the case in which matrix diffusion is not considered, a factor of 3.3 decrease in travel time is observed when matrix diffusion is included (1000 divided by 300). In the 100 fracture scenario contaminant breakthrough times are about 30 percent faster for the strain altered simulations (1100 divided by 830).

Sensitivity to Chemical Retardation

To illustrate the sensitivity of radionuclide transport to chemical (i.e., K_d) retardation the results from three simulations are presented in Figure 4-30. These results are from scenarios involving 10 fractures in which: 1) physical and chemical retardation are inactive, 2) physical retardation is active but chemical retardation is not, and 3) both physical and chemical retardation are active. The modeling results indicate that it would take approximately 30 years for radionuclide breakthrough to occur at the land withdrawal boundary if physical and chemical retardation are not considered. This arrival time increases to about 1000 years (Table 4-13) once matrix diffusion is included.

To facilitate an evaluation of the effects of chemical retardation on radionuclide transport the results from selected simulations are presented in Figure 4-31 and Table 4-13. From these

Figure 4-29. Heterogeneous Hydraulic Conductivity Simulations with Physical Retardation.

Table 4-12. Selected Results from Heterogeneous Hydraulic Conductivity Simulations with Physical Retardation

10 Fractures			
Simulation	Strain	Diffusion	Time (Yr) to Reach 1.00E-05
10T	No	No	30
10TD	No	Yes	1000
10TS	Yes	No	10
10TDS	Yes	Yes	300

100 Fractures			
Simulation	Strain	Diffusion	Time (Yr) to Reach 1.00E-05
100T	No	No	35
100TD	No	Yes	1100
100TS	Yes	No	25
100TDS	Yes	Yes	830

data it is apparent that the inclusion of chemical retardation results in approximately a 2.7 decrease in the travel time. As was mentioned previously, since the R_F is linearly related to the radionuclide velocity it is not surprising that an R_F of 2.7 leads to travel times that are approximately 2.7 times longer than for a comparable simulation in which only matrix diffusion is considered.

A comparison of strained versus *un*strained values for the 10 fracture scenario indicates that, as in the other cases that have been considered, a factor of 3.4 decrease in travel time still holds when chemical retardation is included (2900 divided by 830). In the 100 fracture scenario, contaminant breakthrough times are about 40 percent faster for the strain altered simulations.

4.3.4.3 Comparison Between Homogeneous and Heterogeneous Simulations

In all cases, the breakthrough times computed by the heterogeneous simulations are faster than for the homogeneous case. This is caused by the pattern of hydraulic conductivity interpolated from the Intera data. The hydraulic conductivity values, as shown in Figure 4-17, are higher in the plume area for the heterogeneous case than the homogeneous value of 7 m/y. The heterogeneous values increase downgradient of the source and to the east.

Figure 4-30. Heterogeneous Hydraulic Conductivity Simulations Comparing the Effects of Physical and Chemical Retardation on Radionuclide Transport Times.

Table 4-13. Selected Results from Heterogeneous Hydraulic Conductivity Simulations with Both Physical and Chemical Retardation.

10 Fractures				
Simulation	Strain	Diffusion	Sorption (K_d)	Time (Yr) to Reach 1.00E-05
10TD	No	Yes	No	1000
10TDR	No	Yes	Yes	2900
10TDS	Yes	Yes	No	300
10TDRS	Yes	Yes	Yes	830

100 Fractures				
Simulation	Strain	Diffusion	Sorption (K_d)	Time (Yr) to Reach 1.00E-05
100TD	No	Yes	No	1100
100TDR	No	Yes	Yes	3100
100TDS	Yes	Yes	No	830
100TDRS	Yes	Yes	Yes	2200

Thus, although the plume travels somewhat farther in response to the conductivity distribution, contaminants also travel much faster. Breakthrough times are between 5 and 25 times faster in the heterogeneous case than in the homogeneous simulations. This effect is greatest for a single fracture with no matrix diffusion and no retardation.

Comparisons between heterogeneous and homogeneous simulations where the hydraulic conductivity has been altered by 0.005% strain yield the same conclusions. Breakthrough times are faster in the heterogeneous field than in the homogeneous field. The magnitude of the differences, however, are not as great as in the unaltered case.

Figure 4-31. Heterogeneous Hydraulic Conductivity Simulation with Physical and Chemical Retardation.

5. Consideration of Other Mining Impacts

In addition to subsidence-induced increased hydraulic conductivity of the Culebra, several other potentially detrimental scenarios were postulated in Section 2 above. These are discussed in the context of the information presented here.

5.1 SOLUTION MINING

As described earlier, solution mining of langbeinite is not technically feasible because the evaporite minerals which surround the ore are more soluble than the ore itself. Attempts to solution mine sylvite have not met with success because of the characteristics of the ore body.

In a recent report (NBM95a) addressing resources at the WIPP site, it was noted that:

> "....all mines have held open the option of using solution mining once their sylvite deposits are fully mined out. The concept would rely on the fact that the open spaces left over from mining would allow ore remaining in the pillars to be recovered. No specific plan has ever been formulated whereby a mine would be intentionally flooded and saturated sylvite brine recovered from boreholes. Solar evaporation would need to be used to concentrate the brine because the solutions would be very dilute." However, the possibility exists that solution mining could be used in the vicinity of the disposal system in the near term. As required by §194.32(c), "performance assessments shall include an analysis of the effects on the disposal system of any activities that occur in the vicinity of the disposal system prior to disposal and are expected to occur in the vicinity of the disposal system soon after disposal. Such activities shall include, but shall not be limited to, existing boreholes and the development of any existing leases that can reasonably be expected to be developed in the near future, including boreholes and leases that may be used for fluid injection activities." The chief chemist (Douglas W. Heyn for IMC Kallium (a local potash producer) provided written testimony to EPA related to the Agency's rulemaking actvities on the DOE Compliance Certification Application for WIPP. Heyn concluded that "the rational choice for extracting WIPP potash ore reserves would be by conventional room and pillar mechanical means" (HEY97).

DOE has also reviewed this issue and concluded that, even if solution mining were conducted, the principle impact would be mine subsidence which has already been accounted for in performance assessment (DOE97).

5.2 CHANGE IN FLOW DIRECTION OF WATER-BEARING MEMBERS IF A VERTICAL HYDRAULIC CONNECTION IS CREATED BY SUBSIDENCE

As discussed in the Section 2, if a hydraulic connection did occur, the result could be a shifting of flow in the Culebra toward the southwest. According to information presented by Reeves et al. (REV91), the current travel path is toward the southeast and entails a distance about 3,600 m from the center of the waste area to the southern boundary of the withdrawn area. If subsidence produced a hydraulic connection between the water-bearing members of the Rustler Formation and flow shifted toward the southwest, then the travel distance could be shortened to 2,415 m which is the shortest distance from the southernmost panel in the waste area to the southern boundary of the land withdrawal area. This would represent a 33% decrease in travel distance to the accessible environment. However, this shift would also move the contaminant travel paths into zones of lower hydraulic conductivities which would result in longer travel times to the accessible environment (REV91).

5.3 FORMATION OF SUBSIDENCE-RELATED SURFACE DEPRESSIONS WHERE WATER COULD ACCUMULATE AND ALTER LOCAL RECHARGE

As noted in Section 3.2.1, the maximum observed surface subsidence over existing potash mines in the area is 1.5 m. Using what are believed to be conservative factors in the subsidence equation from Section 3.1.2, including an extraction ratio 90%, a mine height of 2.6 m (8.5 ft), and a subsidence factor of 0.67, the calculated surface subsidence would be 1.6 m. Subsidence of this order is less than the quoted surface relief in the area of 3 meters. Thus, topographical depressions where significant surface water could accumulate and significantly alter local recharge are not likely.

5.4 INCREASED HYDRAULIC GRADIENT IF SIGNIFICANT FLOW FROM WATER-BEARING STRATA INTO MINE WORKINGS OCCURS

Flow of water from the Culebra and Magenta members of the Rustler Formation into open shafts has been observed for all four shafts at the WIPP site (CAU90). Leakage into shafts of various area potash mines has also been reported (CAU90). Quoted leakage values for

the open WIPP shafts are:

- construction and salt handling shaft - 0.019 to 0.11 l/s (599.0-3469.0 m^3/yr)
- waste handling shaft - 0.019 to 0.038 l/s (599.0-1198.0 m^3/yr)
- exhaust shaft - 0.026 to 0.030 l/s (820.0-946.0 m^3/yr)
- air-intake shaft - 0.030 to 0.056 l/s (946.0-1766.0 m^3/yr)

Flows of this magnitude would not persist if the shafts can be adequately sealed after mining operations have ceased or once the formation is dewatered. The Bureau of Land Management does not currently have in place specific regulations for sealing abandoned mine shafts in the KPLA. Rather, abandonment procedures are initiated by the mining companies and the sealing plans are developed on a case by case basis with the BLM (GRI96, CRA96). For example, a current operation involves local removal of the shaft liner and replacement with a concrete plug which extends from the top of the Salado Formation to the bottom of the Culebra member of the Rustler Formation. The plug is 16 to 30 feet in length. The water bearing formations above the plug will be sealed by grouting to prevent the buildup of water on the top of the plug. Procedures for future sealing operations may be different. There is no available evidence as to the longevity of these types of seals. It is reasonable to assume, however, that even degraded seals would impede flow into the shafts.

Since it is not clear that currently contemplated shaft seals will prevent leakage for long periods, it is necessary to consider the impacts of leakage on hydraulic gradients and travel times to the site boundary. To investigate the potential impacts that mining operations may have on groundwater gradients and subsequent contaminant migration rates, a two-dimensional modeling analysis was performed. The analysis assumes that the system is confined and under steady-state conditions. The model also assumes that all groundwater flow is horizontal and occurs within the matrix (i.e, unfractured flow). The Culebra is represented as a homogeneous and isotropic porous medium at a constant thickness of 7.7 m, and an effective porosity of 13.9 percent. A series of simulations were performed in which the hydraulic conductivities (K) were varied from 7 to 500 m/yr to reflect their potential impact on altering contaminant migration rates (Table 5-1).

Since the rate at which radionuclides are transported by groundwater is directly proportional to the hydraulic gradient, any perturbances to the gradient will have a commensurate effect on migration rates. Furthermore, depending upon location, the presence of mining shafts in the vicinity of WIPP could have either a beneficial or detrimental effect on the performance

assessment. Shafts located up gradient from a hypothetical human intrusion (i.e., borehole) would tend to lower or even possibly reverse the hydraulic gradients, thus, reducing the contaminant velocities and subsequent radionuclide releases at the WIPP land withdrawal boundary. Alternatively, shafts located down gradient from an intrusion would result in increased gradients towards the shaft which would tend to accelerate groundwater velocities.

Table 5-1. Summary of Results for Mine Shaft Leakage Scenario

Hydraulic Conductivity (m/y)	Time to Travel 2 km without Shaft (yr)	Groundwater Velocity without Shaft (m/y)	Time to Travel 2 km with Shaft (yr)	Groundwater Velocity with Shaft (m/y)	Flow rate into Shaft (m^3/y)
7	12400.0	0.16	9800.0	0.2	161.0
20	4350.0	0.459	3430.0	0.583	460.0
50	1750.0	1.14	1370.0	1.45	1150.0
500	175.0	11.4	137.0	14.45	11500.0

The shortest distance from the southernmost panel of the WIPP repository to the WIPP land withdrawal boundary is due south, approximately 2400 m. The ambient groundwater gradient also has a strong southerly component. Therefore, for this modeling exercise, the hypothetical mine shaft is located 2000 m down gradient from the waste disposal area. This distance was selected to maximize the effects that would occur if the groundwater gradients were affected by mining; in that the mine shaft is not so far away as to have little effect on flow, yet it is not so close as to create a zone of influence in which contaminants flowing past the mine shaft would actually travel slower due to the diminishing gradient effects that will occur down gradient of the mine shaft.

To maximize the effect that the mine could have on the hydraulic gradients, the drawdown at the mine was set almost at the base of the Culebra at 7.7 m, leaving a seepage face of 0.1 m at the shaft. The flow rate due to this drawdown was then computed by the model (Table 5-1). For example, where K = 7 m/yr, the calculated flow rate is 161 m^3/yr. Because the drawdown was maximized, this value represents a reasonable upper bound for the volume of water that would flow into the open shaft at a Culebra transmissivity (hydraulic conductivity multiplied by unit thickness) of 53.9 m^2/yr.

The hydraulic gradient was also computed at selected points up gradient of the hypothesized mine shaft and compared to the ambient gradient of 0.0032 under current non-mining

conditions. Since the functional relationship between drawdown and transmissivity can be linearly extrapolated to any value of hydraulic conductivity, the overall effect on gradients that is imposed by varying hydraulic conductivities is virtually identical. To illustrate this relationship, the ratio of the gradient under mining conditions to the original gradient of 0.0032 was computed and is shown on Figure 5-1.

To investigate the effect that this change in gradient would have on migration rates, a particle-tracking analysis was performed. This type of analysis moves a particle at the same velocity as the groundwater and the rate is not affected by dispersion, diffusion, or retardation. The results from this travel time analysis are presented in Table 5-1.

In each case, the contaminant would travel approximately 27% faster over the 2000 m distance when the hydraulic gradient is affected by a mine shaft placed in a location chosen to represent mining's maximum expected effect on the hydraulic gradients. The increase for each of the simulations 27% above velocities calculated at ambient gradients and is shown in column 5 of Table 5-1. This increase is small when compared to changes in velocity due to potential increases in the hydraulic conductivity. As required by the rule, hydraulic conductivities will be increased by up to a 1000 fold above their current measured values. To place this travel time change caused by the mine shaft in perspective, groundwater velocities for each of the simulations have been recalculated using hydraulic conductivities that range from 2 to 1000 times their original values and are shown in Table 5-2. In each example, the lowest values for the recalculated velocities fall well above the velocity values that are increased by 27% due to the change in gradient. This velocity comparison indicates that increases in hydraulic conductivity over the range specified by EPA have far greater potential effects on groundwater velocities than increases in the velocities caused by altered hydraulic gradients due to mine shaft leakage. In light of the EPA requirement that DOE perform analyses that are more stringent in evaluating mining effects than those associated with an increase in gradient, it is reasonable to assume that the consequences a 27% decrease in travel time will have on the overall performance assessment will be captured by those additional analyses.

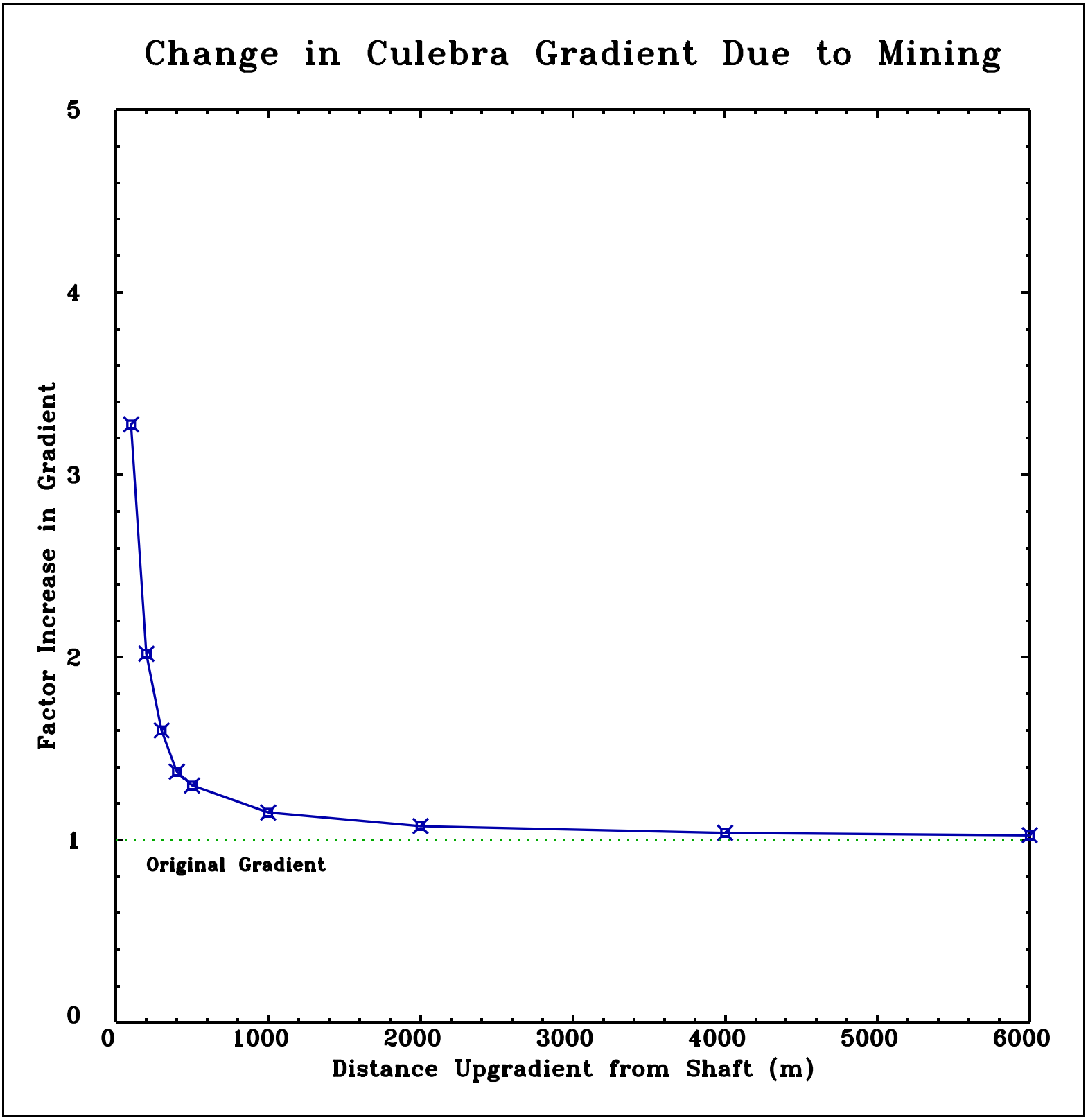
Change in Culebra Gradient Due to Mining
Factor Increase in Gradient
5
4
3
2
1
0
Original Gradient
0
1000
2000
3000
4000
5000
6000
Distance Upgradient from Shaft (m)

Figure 5-1. The ratio of the hydraulic gradient imposed by mining to the ambient gradient.

Table 5-2. Groundwater Velocities at Hydraulic Conductivities Ranging from 2-1000 Times Those Values Presented in Table 5-1.

Hydraulic Conductivity (m/y)	Groundwater Velocity (m/y)
14.0-7000	0.32-161.0
40.0-20,000	0.92-460.0
100.0-50,000	2.30-1151.0
1000.0-500,000	23.0-11510.0

5.5 DAMAGE TO BOREHOLE OR SHAFT SEALS BY SUBSIDENCE

From the information supporting Figure 1-2, it can be shown that the closest approach of the sylvite reserves (a grade x thickness product of 40) to waste shaft is slightly over 2,500 feet. The top of this sylvite ore zone (the 10th) lies about 1,900 feet below the surface (GRI95). Based on a 45^{o} angle of draw, the impacted area from mining the BLM lease grade reserves would be about 600 feet from the waste shaft at the surface and at proportionately greater distances below the surface where maintenance of the shaft seal is more important (e.g., through the Rustler Formation). Alternatively, if one assumed the most pessimistic angle of draw (58^{o}) reported for the area in ITC94, the maximum extent of the impacted area would be 3,040 feet and the disturbed zone would intersect the waste shaft at about 340 feet below the surface. The juncture is still some 200 feet above the top of the Rustler Formation and thus shaft seals should not be affected at any critical location in transmissive members of this formation.

If all the BLM lease grade reserves within the land withdrawal area were mined out, a number of boreholes would be undercut by the mining operations and the sealed area of the borehole subject to subsidence-induced strains. However, the borehole seals between the repository and the mine workings should not be affected by the mining operations[15].

[15] Inside the withdrawn area, only four boreholes associated with the WIPP Project (WIPP 12, 13, DOE 1, and ERDA 9) and two earlier oil and gas holes reached or exceeded the depth of the repository.

Thus, it is not expected that mining would breach shaft seals at any critical point along the sealed length and would not affect borehole seals between the repository horizon and the mine workings (about 430 feet). Consequently, pathways would not be opened to the repository by a mining related seal failure mechanism which would facilitate release of radionuclides.

5.6 INCREASED HYDRAULIC CONDUCTIVITY OF THE SALADO FORMATION DUE TO EXCAVATION-INDUCED STRESSES

As discussed in Section 3.1.2, the maximum increase in the hydraulic conductivity of the Salado Formation due to stress redistribution around underground openings is expected to be about an order of magnitude and this altered conductivity decreases rapidly as one moves away from the mined opening. At a distance equal to six times the width of the opening, the altered conductivity is only twice that of undisturbed salt. Even with changes of this magnitude, the salt would remain highly impermeable. In addition, creep should cause the salt to revert to near the undisturbed state.

6. Comparison with CCA

As mentioned previously, EPA's approach to the evaluation of mining impacts was to identify probable maximum effects *via* a bounding analysis. Since DOE has provided a reasonable argument for the presence of matrix diffusion and chemical retardation within the Culebra the most relevant and potentially realistic results of the STAFF3D mining analysis are shown in Table 4-13. These results indicate that for 10 fractures the contaminant velocities in the mined scenarios are about 3.5 times faster than for the unmined scenarios. The assumption of 10 fractures is a reasonable assumption, since the work by Holt (1997) suggests that in many areas the fractures in the Culebra are so closely spaced that the unit behaves as a single porosity medium. As shown in the PAVT (Docket: A-93-02, V-G-26 and V-G-28), it would take significantly higher changes to the radionuclide velocities in the Culebra before this pathway becomes a major contributor to releases. The conservative nature of the STAFF3D assumptions are discussed with respect to DOE's more realistic approach taken in the CCA below.

Mined Area. DOE stated that the only natural resource currently being mined near the WIPP is potash (potassium salts) within the McNutt member of the Salado Formation (Docket: A-93-02, II-G-01,Chapter 6.4.6.2.3, p. 6-137). Consistent with 194.32(b), DOE therefore only considered potash mining in the performance assessment.

Based upon information presented in Appendix MASS.15 (Docket: A-93-02, II-G-01) , DOE concluded that only Zones 4 and 10 of the McNutt member are currently economically minable. The 4th ore zone is nearest to the proposed waste panel horizon; it lies about 300 feet (100 meters) above the proposed waste panel horizon. DOE outlined the extent of the horizons of both Zones 4 and 10 within and outside of the controlled zone in the CCA. DOE indicated that Zones 4 and 10 occur in a north-south trend along the eastern third of the controlled area. Outside of the controlled area, they occur in an area to the immediate southeast of the WIPP Site Boundary. However, DOE indicated that potash resources occur and are expected to be mined within the Culebra groundwater modeling domain area, which extends to the south of the controlled area. DOE also noted that no minerals are present in minable quantities or types similar to those currently being mined in the Delaware Basin, in units above the Salado Formation (Docket: A-93-02, II-G-01, Chapter 6.4.6.2.3, p. 6-136 to 6-147).

During the process of mining, effects of the mining on overlying geologic units extend beyond

the mined area. DOE used the concept of 'angle of draw' to identify the area in the Culebra dolomite in which the Culebra's hydraulic conductivity would be affected by mining. DOE assumed that the angle of draw (the angle 'outward and upward' from the mined area that will be impacted by mining) is 45 degrees. DOE considered the effects of mining within and around the controlled area under the disturbed case for the PA, while effects outside of the controlled area were considered under the undisturbed case.

Boundary Conditions. The CCA used a regional model to assess the impacts of mining (Docket: A-93-02, II-G-01,Chapter 6.4.6.2.3, p. 6-139, Figure 6-19). Alternatively, the STAFF3D modeling used a more local approach as presented in Section 4.3.3 of this TSD. Since no attempt was made in the STAFF3D simulations to recalculate the hydraulic boundary conditions under the mining scenarios (i.e., gradients should become flatter because of the higher transmissivites), the hydraulic gradients would be maximized. Therefore, the differences in the contaminant velocities between the mining vs non-mining scenarios would be accentuated.

Physical Properties. The effect of mining on the Culebra dolomite's hydraulic conductivity in the CCA was incorporated by multiplying location-specific values in the Culebra transmissivity field by a randomly sampled value from one to 1,000 within areas identified by DOE to be impacted by mining. Changes in hydraulic conductivity were therefore the same or higher due to mining. DOE indicated that every Latin Hypercube sample (LHS) vector and every steady state flow field used in Culebra transport simulations incorporated this change to the transmissivity field. The code ALGEBRA was used to apply the effects of potash mining to the GRASP_INV tranmissivity fields (Docket: A-93-02, II-G-01, Chapter 6.4.6.2, p. 6-123 to 6-133), in the performance assessment.

As shown in Table 4-5 of this TSD, the strain altered vs unaltered equivalent hydraulic conductivities, used in the STAFF3D analyses range from about 1 to a little over 170. These predicted changes are based on parallel plate theory that maximizes the effects because all of the strain is assumed to be placed on the fractures. Therefore, DOE's use of a multiplication factor of up to 1,000 is adequate.

7. Summary

Extensive potash mining operations are being conducted in the vicinity of the WIPP site with current mine workings less than 1.5 miles from the site boundary (DOE95). Existing potash border abut the site boundary around much of its perimeter (SIL94) and its is expected that current mining operations will be extended to the land withdrawal boundary.

Reserves and resources of both sylvite and langbeinite exist within the land withdrawal boundary. Based on current BLM lease grade standards (four feet of 4% K_2O for langbeinite and four feet of 10% K_2O for sylvite), the langbeinite reserves are within 3,490 feet of the waste repository footprint and sylvite reserves are within 1,330 feet of the footprint. These reserves cannot be exploited currently because the WIPP LWA prohibits mining within the withdrawn area.

At some time in the future, after active institutional controls are no longer practicable and, if passive institutional controls have failed to warn about the buried hazards, it is a conceptual possibility that mining of the ore remaining within the withdrawn area could occur. Such a hypothetical mining operation would probably require development of a new infrastructure since existing reserves outside the withdrawn area would likely have been depleted prior to the failure of institutional controls.

The most likely detrimental impact of such future mining would be increased hydraulic conductivity of the Culebra Member of the Rustler Formation resulting from subsidence-induced fracturing of the relatively brittle dolomite. This fracturing (or widening of existing fractures) could reduce the lateral transit time for radionuclides to the accessible environment. The increased hydraulic conductivity is of no consequence unless a hydraulic connection exists between the Culebra and the repository 1,440 feet below. Based on current WIPP scenarios, the hydraulic connection could be created by an inadvertently drilled borehole which intersected the repository. Thus performance assessment will need to address the probability and consequence of such a combination of events. Based on studies reviewed here, it does not appear that other mining-related scenarios will have significant detrimental effects on the natural and man-made barriers protecting the repository.

Simulation of full extraction mining of 10 ft of potash at a depth of about 1,500 ft near the

WIPP shows vertical tensile strains over the mined panel and slowly decreasing horizontal tensile strains beyond the panel edge. Although generally in the elastic range, the strains, when integrated between assumed fractures, lead to displacements that are significant relative to reasonable fracture apertures. This, in turn, can increase the fracture hydraulic conductivity of the Culebra.

Building on the rock mechanics analysis, a series of STAFF3D flow and transport simulations are presented that investigate the effect of increased hydraulic conductivity caused by collapse of underground mining operations in the vicinity of the WIPP site. These simulations were conducted in a sensitivity analysis that included the number of fractures in the Culebra, matrix diffusion, chemical retardation, and degree of heterogeneity in the hydraulic conductivity field. Each sensitivity simulation compared the breakthrough of plutonium at the downgradient WIPP site boundary between the current hydraulic conductivity in the Culebra and the increased hydraulic conductivity that would result from a strain of 0.005 percent. The strain value was estimated based on modeling the collapse of a hypothetical underground mine at WIPP. The following summarizes the approach and the primary conclusions obtained from this study.

The STAFF3D modeling assumes that flow in the Culebra occurs through a series of horizontal fractures. Simulations were conducted for 1, 10, and 100 fractures. The equivalent porous medium hydraulic conductivity of 7 m/y was maintained in all cases, except for the strain-induced conductivity fields. Modeling results show that as the number of fractures increases, the difference between the unstrained and strained hydraulic conductivity fields becomes less. In the case where hydraulic conductivity is homogeneous with no matrix diffusion and no retardation, travel times are factors of 55, 4.2, and 1.7 times faster in the strained model for 1, 10, and 100 fractures, respectively. It is unlikely, however, that the strain imposed by mining would increase the velocities by more than a factor of 5 due to the conservative assumptions inherent in the STAFF3D modeling.

When matrix diffusion is added to the model simulations, the radionuclide travel times to the downgradient boundary are decreased significantly. In the case where hydraulic conductivity is homogeneous and matrix diffusion is included but not retardation, travel times are factors of 38, 5.0, and 1.5 times faster in the strained model for 1, 10, and 100 fractures respectively. These simulations indicate that the results are insensitive to the magnitude of the diffusion coefficient (in the range reported in the 1992 PA) for the 10 and

100 fracture cases.

Adding chemical retardation *via* a retardation factor of 2.75 slows the travel times even further. The relative impact of strain induced conductivities, however, is the same as for the case where matrix diffusion is simulated without chemical retardation. The chemical retardation slows the travel times by a factor equal to the retardation factor, i.e., 2.75.

Similar conclusions were obtained for the case where the hydraulic conductivity distribution is heterogeneous. The differences between the 1, 10, and 100 fracture scenarios, however, are not as great as in the homogeneous simulations. Overall, breakthrough times are 5 to 25 times faster in the heterogeneous than in the homogeneous simulations due to the fact that the hydraulic conductivity values were much higher than the homogeneous value of 7 m/y in the area of the hypothetical contaminant source.

8. References

AXN94 Axness, C. et al., "Non-Salado Flow and Transport Position Paper," (Revision 1) Sandia National Laboratories, December 15, 1994.

BAI94 Bai, M. and D. Elsworth, "Modeling of Subsidence and Stress-Dependent Hydraulic Conductivity for Intact and Fractured Porous Media," in Rock Mechanics and Rock Engineering, v. 27, no. 4, pp. 209-234, 1994 (U.S. Office of Surface Mining and Reclamation Enforcement, West Virginia University).

BAR93 Barker, J.T. and G. S. Austin, "Economic Geology of the Carlsbad Potash District, New Mexico," in New Mexico Geological Society Guidebook, 44th Field Conference, New Mexico and West Texas, pp 283-291, 1993.

BLM93 U.S. Bureau of Land Management, "Preliminary Map Showing Distribution of Potash Resources", Carlsbad Mining District, Eddy & Lea Counties, New Mexico, Roswell District, 1993 (U.S. Department of Interior, Bureau of Land Management, Roswell, NM).

BOO92 Booth, C. J., "Hydrologic Impacts of Underground (Longwall) Mining in the Illinois Basin," in Proceedings of Third Workshop on Surface Subsidence Due to Underground Mining, pp 222-227, 1992 (U.S. Office of Surface Mining and Reclamation Enforcement, West Virginia University).

CAU90 Cauffman, T.L., A.M. LaVenue, and J.P. McCord, "Ground-Water Flow Modeling of the Culebra Dolomite, Volume II: Data Base," Intera, Inc., SAND89-7068, October 1990 (Docket: A-93-02, II-G-1, Ref. #115).

CHE78 Cheeseman, R.J., "Geology and Oil/Potash Resources of Delaware Basin, Eddy and Lea Counties, New Mexico," in New Mexico State Bureau of Mines and Mineral Resources Circular 159, 1978.

CON95 Cone, L. M., Letter dated October 12, 1995 from U.S. DOI/BLM District Manager to G. B. Griswald.

CRA96 Cranston, C., Bureau of Land Management, Carlsbad NM, Private Communication to J. Channell, S. Cohen and Associates, Inc., January 17, 1996 (Docket: A-93-02, II-G-1, Ref. #238).

DAP82 D'Appolonia Consulting Engineers, Inc., "Natural Resources Study - Waste Isolation Pilot Plant (WIPP) Project, Southeastern New Mexico," Draft Report, Project No. NM78-648-813A, January 1982.

DOE80 U.S. Department of Energy, "Final Environmental Impact Statement - Waste Isolation Pilot Plant," U.S. DOE/EIS-0026, October 1980 (Docket: A-93-02, II-G-1, Ref. #178).

DOE93 U.S. Department of Energy, "Implementation of the Resource Disincentive in 40 CFR Part 191.14(e) at the Waste Isolation Pilot Plant," DOE/WIPP 91-029, Revision 1, June 1993.

DOE95 U.S. Department of Energy, "Draft Title 40 CFR 191 Compliance Certification for the Waste Isolation Pilot Plant," Draft-DOE/CAO-2056, March 31, 1995.

DOE97 DOE's Response to EEG's Letter of February 7, 1997 dated March 13, 1997, see Hicks (1887a). (Docket: A-93-02, II-H-24).

DUP94 Dupree, J.A. and R.W. Eveleth, "New Mexico Annual Report - 1992," U.S. Bureau of Mines, February 1994. (U.S. Department of Interior/U.S. Geological Survey Library, telephone [703] 648-4000).

ELS95 Elsworth, D. and J. Liu, "Topographic Influence of Longwall Mining on Ground-Water Supplies," in Ground Water, vol. 33, no. 5, pp. 786-793, September-October 1995. (U.S. Department of Interior/U.S. Geological Survey Library, telephone [703] 648-4000).

EPA96 U.S. Environmental Protection Agency, Criteria for the Certification and RE-Certification of the Waste Isolation Pilot Plant's Compliance with the 40 CFR Part 191 Disposal Regulations, "EPA 402-R-96-002, January 1996." (Docket: A-93-02, II-G-1, Ref. #239).

GAL82 Gale, J.E., "Assessing the permeability characteristics of fractured rock," in Recent Trends in Hydrogeology, Geological Society of America, Special Paper 189, ed., p. 163-181, 1982. (U.S. Department of Interior/U.S. Geological Survey Library, telephone [703] 648-4000).

GAL94 Galson, Daniel A. (compiler), "Assessment of Future Human Actions at Radioactive Waste Disposal Sites," report of an NEA Working Group, 9203b-2, Version 5.2, April 11, 1994.

GRI82 Griswold, George B., "Geologic Overview of the Carlsbad Potash-Mining District," in Industrial rocks and minerals of the Southwest, compiled by George S. Austin, New Mexico Bureau of Mines and Mineral Resources Circular 182, 1982. (State of New Mexico, New Mexico Bureau of Mines and Mineral Resources, Telephone [505] 255-8005)

GRI95 Griswold, G.B. "Method of Potash Reserve Evaluation," in reference NMB95.

(Docket: A-93-02, II-G-1, Ref. #460).

GRI96 Griswold, George B., Private Communication to J. Channell, S. Cohen and Associates Inc., January 17, 1996. (Docket: A-93-02, II-G-1, Ref. #239).

HEY97 Letter from Douglas W. Heyn, IMC Kallium to EPA dated February 28, 1997 Re: Potash Solution Mining on WIPP Reservation. (Docket: A-93-02, II-H-19).

HUN89 Hunter, R.L., "Events and Processes for Constructing Scenarios for the Release of Transuranic Waste from the Waste Isolation Pilot Plant, Southeastern New Mexico," Sandia National Laboratories, SAND89-2546, December 1989. (Docket: A-93-02, II-G-1, Ref. #321).

ITC94 IT Corporation, "Backfill Engineering Analysis Report," August 1994. (Docket: A-93-02, II-G-1, Ref. #684).

KEL91 Kelleher, J.T., et al., "Overburden Deformation and Hydrologic Changes Due to Longwall Coal Mine Subsidence on the Illinois Basin," in Proceedings of Fourth International Symposium on Land Subsidence, pp. 195-204, May 1991. (Illinois State Geological Survey-IAHS Pub. No. 200, 1991)

LAM78 Lama, R.D. and V.S. Vutukuri, Handbook on Mechanical Properties of Rocks, Vol. II, Trans Tech Publications, pp 342-344 & 411, 1978.

MAT92 Matetic, R.J. and M.A. Trevits, "Hydrologic Variations Due to Longwall Mining," in Proceedings of Third Workshop on Surface Subsidence Due to Underground Mining, pp 204-213, 1992. (U.S. Bureau of Mines, Pittsburg Research Center).

NBM95a New Mexico Bureau of Mines and Mineral Resources, "Evaluation of Mineral Resources at the Waste Isolation Pilot Plant (WIPP) Site," Volume 2, Chapters III - VIII, March 31, 1995. (Docket: A-93-02, II-G-1, Ref. #460).

NEA92 Nuclear Energy Agency, "Systematic Approaches to Scenario Development," Organization for Economic Co-operation and Development, Paris 1992. (Docket: A-93-02, II-G-1, Ref. #488).

NMB95 New Mexico Bureau of Mines and Mineral Resources, "Evaluation of Mineral Resources at the Waste Isolation Pilot Plant (WIPP) Site," Volume 1, Executive Summary, NM.BMMR-95*1020, March 31, 1995. (Docket: A-93-02, II-G-1, Ref. #460).

OCC88 Oil Conservation Commission, "Case No. 9318, Order No. R-111-P," Energy, Minerals and Natural Resources Dept., State of New Mexico, April 21, 1988. (Docket: A-93-02, II-G-1, Ref. #462).

PAR78 Pariseau, W.G. "Interpretation of Rock Mechanics Data", Vol. I & II, U.S. Bureau of Mines Contract Report, Contract No. H0220077, 1978. (U.S. Department of Interior/U.S. Geological Survey Library, telephone [703] 648-4000).

PAR91 Pariseau, W.G. "Using Utah2/PC", U.S. Bureau of Mines - U of Utah Workshop on Personal Computer Finite Element Modeling for Ground Control and Mine Design Notes, Denver, Colorado, 1991. (U.S. Department of Interior/U.S. Geological Survey Library, telephone [703] 648-4000).

POW78 Powers, D.W., et al. "Geological Characterization Report, Waste Isolation Pilot Plant (WIPP) Site, Southeastern New Mexico," ed. Sandia National Laboratories, SAND78-1596, August 1978. (Docket: A-93-02, II-G-1, Volume IX, Appendix GCR).

REV91 Reeves, M. et al., "Regional Double-Porosity Solute Transport in the Culebra Dolomite Under Brine-Reservoir-Breach release Conditions: An Analysis of Parameter Sensitivity and Importance," Sandia National Laboratories, SAND89-7069, 1991. (Docket: A-93-02, II-G-1, Ref. #542).

SAN92 Sandia National Laboratories, "Preliminary Performance Assessment for the Waste Isolation Pilot Plant, December 1992," SAND92-0700 (Vol. 3), December 1992. (Docket: A-93-02, II-G-1, Ref. #563).

SEE78 Seedorff, W.A., "Resource Study for the Waste Isolation Pilot Plant Site, Eddy County, New Mexico," AIM Inc., August 15, 1978.

SIL94 Silva, M.K., "Implications of the Presence of Petroleum Resources on the Integrity of the WIPP Site," EEG-55, New Mexico Environmental Evaluation Group, June 1994. (Docket: A-93-02, II-G-1, Ref. #592).

SMI73 Smith, G.I.,et al., "Evaporites and Brines," in United States Mineral Resources, Donald A. Brobst and Walden P. Pratt, ed., U.S. Geological Survey Professional Paper 820, 1973. (U.S. Department of Interior/U.S. Geological Survey Library, telephone [703] 648-4000).

SNO69 Snow, D.T. "Anisotropic permeability of fractured media," in Water Resources Research, vol. 5, no. 6, p. 1273-1289, 1969. (U.S. Department of Interior/U.S. Geological Survey Library, telephone [703] 648-4000).

USG88 U.S. Geological Survey, "Ground-Water Hydrology of Marshall County, West Virginia, with Emphasis on the Effects of Longwall Coal Mining," Water Resources Investigations Report 88-4006, 1988. (U.S. Department of Interior/U.S. Geological Survey Library, telephone [703] 648-4000).

WEI79 Weisner, R.C., et al., "Valuation of Potash Occurrences Within the Nuclear Waste Isolation Pilot Plant Site in Southeastern New Mexico," U.S. Bureau of Mines Information Circular 8814, 1979. (U.S. Department of Interior/U.S. Geological Survey Library, telephone [703] 648-4000).

APPENDIX A
BREAKTHROUGH CURVES FOR EACH STAFF3D SIMULATION